THE DEVELOPMENT OF A THERAPEUTIC PLATFORM TO ENHANCE THE ACTIVITY AND PERSISTENCE OF CHIMERIC ANTIGEN RECEPTOR (CAR)-T CELL

RESEARCH PAPER

Bachelor programme

Medical and Pharmaceutical Biotechnology

by

Almira SLAMNIK

Acknowledgments

I extend my deepest gratitude for the invaluable support and guidance provided by my supervisor, Shreya Mantri, BSc, currently a Ph.D. student in the Rashidian Lab. I would also like to express my thanks to Mohammad Rashidian, Ph.D., Assistant Professor, for his insightful feedback on experimental designs and continuous guidance throughout this research journey. Special appreciation goes to Leila Munaretto, MSc, and Harris Allen for their invaluable assistance with experiments.

I am particularly grateful to the Marshall Plan Foundation for their generous financial support during my stay in Boston. Without this funding, the realization of this research endeavor would not have been possible.

Abstract

This research presents a meticulous analysis of the CAR-Enhancer (CAR-E), a novel therapeutic platform designed to augment the effectiveness of CAR-T cell therapy. In-depth in vitro characterizations of CAR-E encompassed thorough examinations of binding efficacy, activation capabilities, proliferation dynamics, and killing potential, with particular attention to potential off-target effects. The study yielded notable observations, elucidating nuanced binding patterns, temporal activation dynamics, and proliferation capabilities, thereby providing a profound understanding of CAR-E behavior.

In addition to comprehensive in vitro assessments, the research extended to in vivo experiments, involving CAR-T cell expansion and challenges with Nalm6 and Raji cells. Results indicated that CAR-E exhibited selective binding affinity to Axicabtagene-ciloleucel (Axicel) and Lisocabtagenemaraleucel (Lisocel), with implications for overall therapeutic performance. Evaluation of CAR-E's activation potential, proliferation capabilities, and killing efficiency contributed valuable insights into its therapeutic relevance. In vivo expansion experiments demonstrated substantial CAR-T cell expansion with Axicel, while challenges with Nalm6 and Raji cells revealed potent tumor clearance and enhanced survival, underscoring the potential clinical impact of CAR-E.

Assessment of off-target effects on non-transduced T cells underscored minimal and transient effects, affirming the favorable safety profile of CAR-E. A detailed discussion of the dose-dependent behavior of CAR-E in the context of potential clinical applications provided crucial insights for optimizing therapeutic interventions. The research concludes with a comprehensive discussion that integrates in vitro and in vivo data, offering a holistic understanding of the functional implications of CAR-E constructs. This study contributes significant insights into the dynamic interplay crucial for advancing the efficacy and safety of CAR-T cell therapies.

Table of Contents

List of Illustrations

List of Tables

List of Abbreviations

ACK … ammonium-chloride-potassium

APS … ammonium persulfate

Axicel … Axicabtageneciloleucel

BCMA … B-cell maturation antigen

BLI … Bio-Luminescent Imaging

BM … bone marrow

Brexucel … Brexucabtageneautoleucel

BSA … Bovine Serum Albumin

CAR … Chimeric Antigen Receptor

CAR-E … Chimeric Antigen Receptor - Engager

Ciltacel … Ciltacabtageneautoleucel

CM1/2 … co-stimulatory molecules 1/2

CRS … Cytokine Release Syndrome

DMEM … Dulbecco's Modified Eagle Medium

DNA … deoxyribonucleic acid

DTTT … dithiothreitol

E:T … Effector: Target

EDTA … Ethylenediamine tetra acetic acid

ELISA … Enzyme-Linked Immunosorbent Assay

FBS … Fetal Bovine Serum

FDA … Food and Drug Administration

FLAG … DYKDDDDK

GFP … Green fluorescent protein

Gy … Gray

HEPES … 1-(2-hydroxyethyl)-1-piperazineethanesulfonic acid

HRP … Avidin-horseradish peroxidase

Idecel … Idecabtagenevicleucel

IFN … interferon

IL … Interleukin

IL2-R-α … IL2-Receptor-α

IL2-R-β … IL2-Receptor-β

IMAC … Immobilized Metal Affinity Chromatography

ITAM … immunoreceptor tyrosine-based activation motif

JAK-STAT … Janus-Kinase-Signal Transducer and activator of transcription

Lck … lymphocyte-specific protein tyrosine kinase

Lisocel … Lisocabtagenemaraleucel

MFI … mean fluorescence intensity

PBMC … Human Peripheral Blood Mononuclear Cell

PBS … phosphate-buffered saline

pSTAT5 … Phosphorylated STAT5

RPMI … Roswell Park Memorial Institute

scFv … single-chain variable fragment

SDS-PAGE … Sodium Dodecyl Sulfate Polyacrylamide Gel Electrophoresis

TCR/CD3 … T cell receptor/cluster of differentiation 3

TEMED … N, N, N’, N'-Tetramethylethylenediamine

Tisacel … Tisagenlecleucel

TMB … 3,3’,5,5’-Tetramethylbenizidine

TNF … tumor necrosis factor

VH … variable heavy chain

VL … variable light chain

1 Introduction

1.1 Cancer

Cancer represents a pathological condition characterized by uncontrolled cellular proliferation and the dissemination of these aberrant cells to distant anatomical sites within the organism. It can originate in various anatomical locations throughout the body, and it stands as a prominent contributor to global mortality. In 2017, the disease accounted for the demise of 9.56 million individuals is cancer, signifying that it is responsible for approximately one-sixth of all deaths worldwide. Among the myriad cancer types, breast and lung cancer emerge as the two most prevalent malignancies, affecting both sexes. In the year 2020, non-Hodgkin lymphoma, with an incidence of 544,352 cases, ranked eleventh in terms of frequency, followed closely by leukemia with 474,519 reported cases. Lymphoma pertains to malignancies originating in lymphocytes, perturbing white blood cell populations, while leukemia originates in the primitive blood-forming cells within the bone marrow and the spongy osseous tissue, and both fall under the category of hematological malignancies.(1–3)

Therapeutic modalities for combating hematological cancer encompass a range of approaches. This includes chemotherapy, immunotherapy, radiation therapy, targeted therapy, bone marrow transplantation, and the increasingly prominent CAR-T cell therapy, which is widely employed in clinical practice.(1)

1.2 CAR-T cell therapy

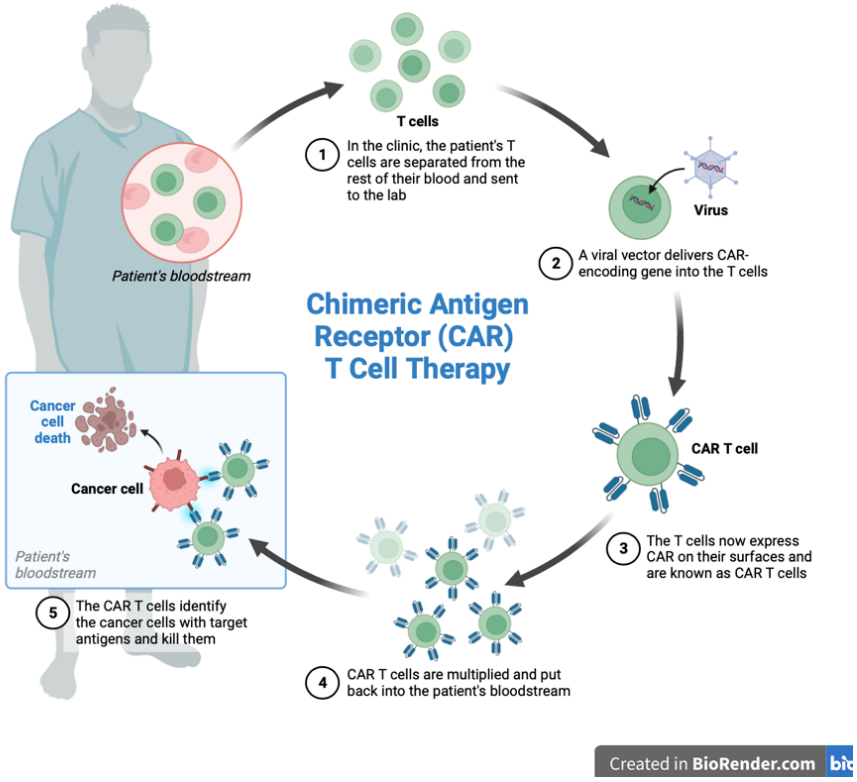

Figure 1: Overview of CAR-T cell therapy

Patients subjected to CAR-T cell therapy initially undergo a phlebotomy procedure to procure a blood sample. Subsequently, the collected blood is subjected to T-cell isolation, followed by their transfer to a controlled laboratory environment. Within this laboratory setting, these T cells are transduced with a viral vector bearing the genetic blueprint responsible for encoding the CAR. The CAR is subsequently expressed on the surface of the T cells through this process. Post-transduction, the CAR-T cell population is systematically expanded until it reaches a therapeutically sufficient quantity, at which point they are reinfused into the patient's bloodstream. Before the CAR-T cells are reinfused, the patient must undergo lymphodepleting chemotherapy. Within the circulatory system, these CAR-T cells adeptly recognize and eliminate cancer cells through their engineered receptors.(4,5)

1.2.1 Mechanism of CAR-T cell therapy

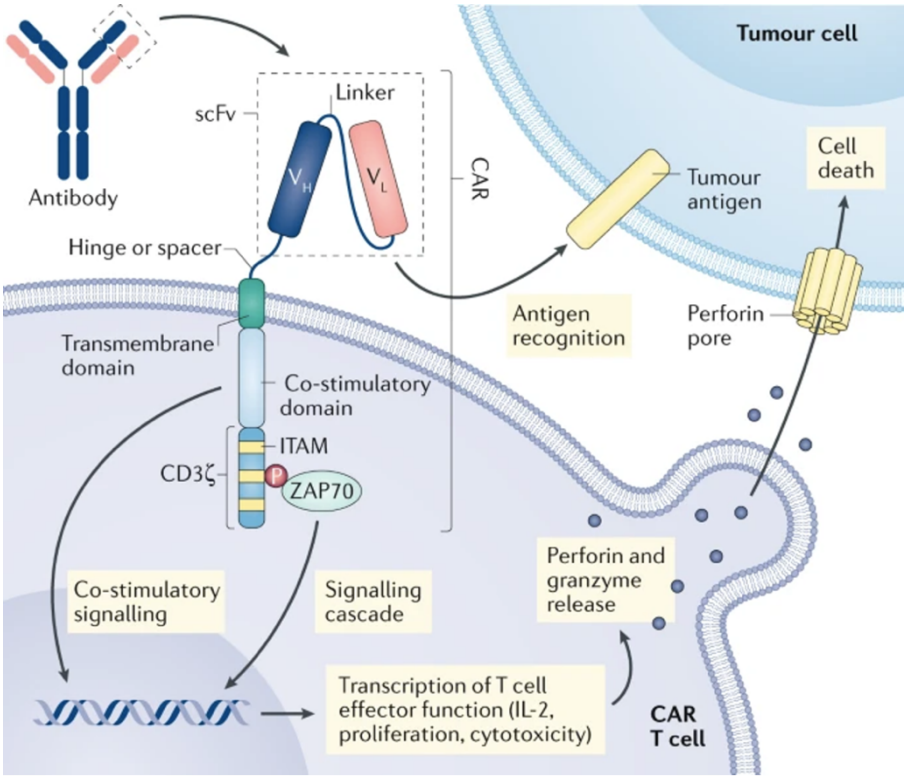

Figure 2: Mechanism of CAR-T cell therapy (7)

The single-chain variable fragment (scFv) within the CAR engages in specific binding interactions with an antigen present on the surface of tumor cells. The scFv region, constituting the antigen recognition component of an antibody, encompasses both a variable heavy chain (VH) and a variable light chain (VL). Upon successful binding of the CAR to the tumor-associated antigen, activation of both the co-stimulatory domain and the signaling domain ensues. This activation cascade initiates transcriptional events, including but not limited to the production of Interleukin (IL) 2 and the induction of various effector functions inherent to T cells. Among these effector functions, the release of cytotoxic molecules such as perforin and granzyme represents a pivotal mechanism through which the CAR-engineered T cell combats the tumor cell, facilitating its eradication. (6,7)

1.2.2 Structure of CAR-T cells

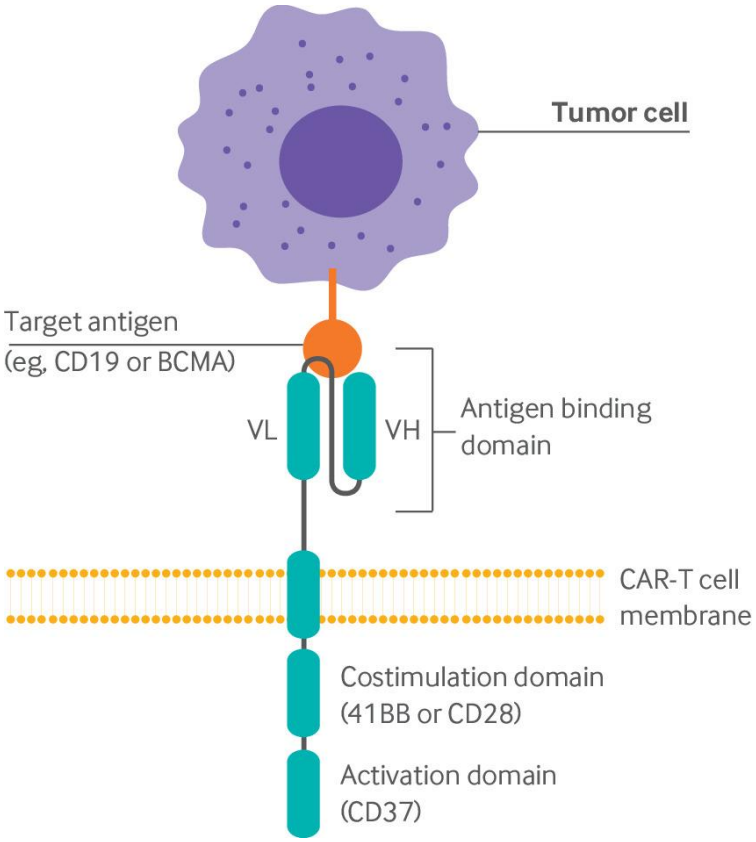

Figure 3: Structure of CAR-T cells (8)

CARs are comprised of several essential structural components, such as a scFv region, a spacer domain, a transmembrane domain, and one or more cytoplasmic domains. Within the cytoplasmic portion of the CAR, the activation domain is embodied by the ζ chain, derived from the T cell receptor/cluster of differentiation 3 (TCR/CD3) complex. This activation domain encompasses three immuno-tyrosine activation motifs (ITAMs), pivotal in transducing signaling events. Signaling initiation occurs through the phosphorylation of these ITAMs, orchestrated by the lymphocyte-specific protein tyrosine kinase (Lck) within the signaling domain. The co-stimulation domain, essential for CAR-mediated signaling, operates through distinct signaling pathways. Activation of this pathway culminates in the physiological activation of T cells, further contributing to CAR-T cell functionality.(7,8)

1.2.3 Generations of CAR-T cells

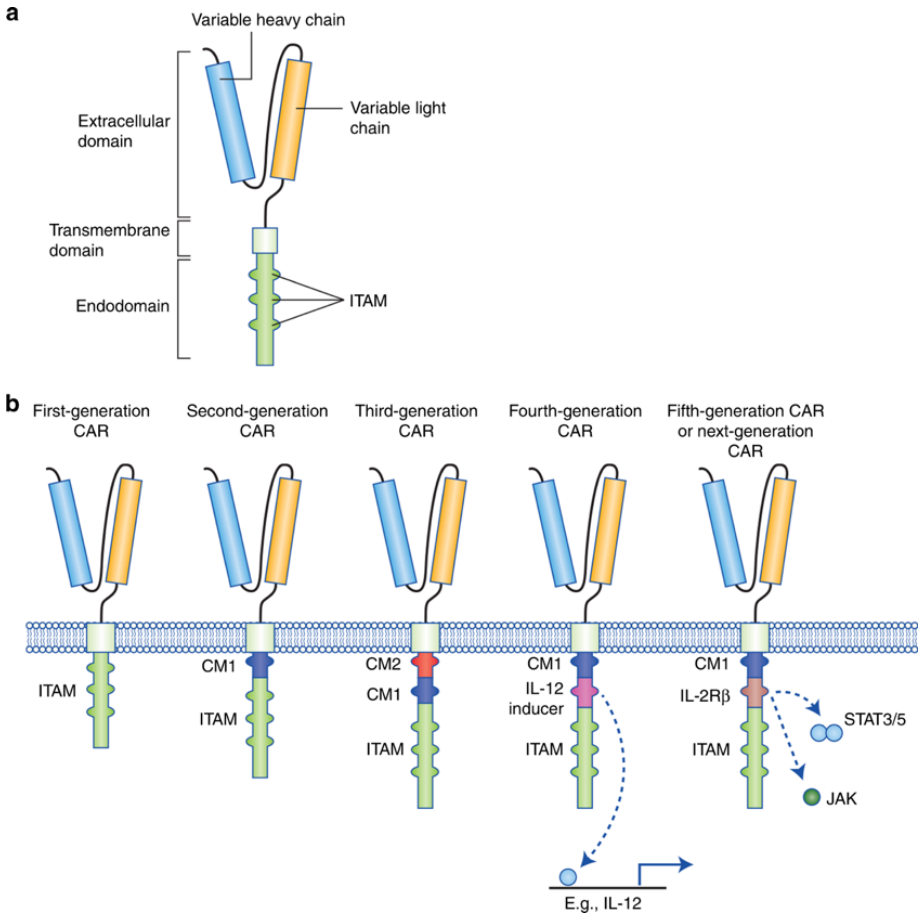

Figure 4: Generations of CAR-T cells (9)

CAR engineering evolved with the inception of first-generation CAR constructs. These initial CARs incorporated the CD3ζ signaling domain, recognized for its capacity to instigate tumor-specific cytotoxicity through ITAMs. Subsequent generations of CARs, namely the second and third generations, integrated additional costimulatory molecules denoted as CM1/2, such as CD28 or 4-1BB. This augmentation contributed to heightened antitumor cytotoxicity, augmented cytokine production, and enhanced proliferation and persistence of CAR-T cells. The fourth generation of CARs, colloquially known as "armored" CARs, introduced a cytokine inducer such as IL12 cytokine inducer. This innovation promoted the release of cytokines that activated innate immune cells against the tumor and concurrently conferred resistance against inhibitory elements within the tumor microenvironment. The fifth generation of CARs bears structural similarities to the second generation but distinguishes itself by incorporating intracellular domains derived from cytokine receptors,

such as the IL-2β chain fragment. This strategic modification induces the activation of the Janus Kinase-Signal Transducer and Activator of Transcription (JAK-STAT) pathway, further enhancing the CAR-T cell response.(5,9,10)

1.3 U.S. Food and Drug Administration (FDA) approved CAR-T cell therapy

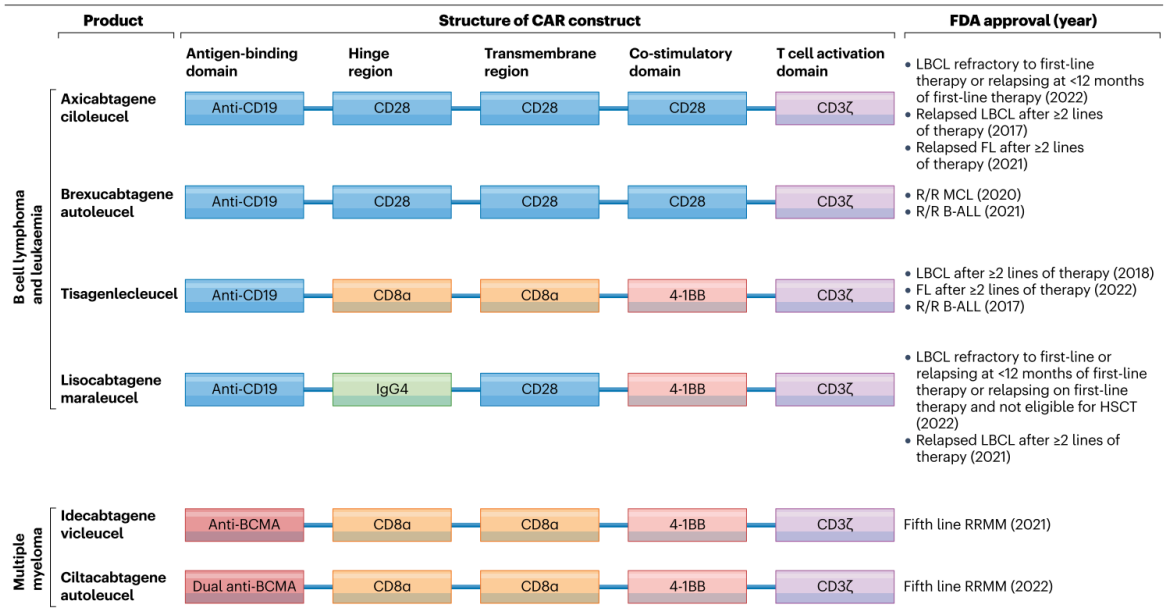

Figure 5: FDA approved CAR-T cells (11)

CARs serve as pivotal molecular tools directing T cell responses toward specific target antigens such as CD19 and BCMA. Notably, CD19 is the designated target antigen for the treatment of relapsed and/or refractory B cell lymphoma and B cell acute lymphoblastic leukemia, follicular lymphoma, and mantle cell lymphoma, whereas BCMA is the antigen of choice for managing relapsed and/or refractory multiple myeloma. CAR-T cell therapy can induce persistent clinical consequences characterized by cytopenia and hypogammaglobulinemia. These conditions are recognized as enduring outcomes resulting from the treatment. CD19-targeted CAR-T cells have received regulatory approval for the treatment of aggressive B cell lymphomas in the relapsed and/or refractory setting. Efficacy assessments from multicenter clinical trials have established a substantial complete response rate, ranging from 71% to 81%. Consequently, this therapeutic modality may be administered as

a standalone treatment or employed as a bridge to allogeneic hematopoietic stem cell transplantation.(11)

Prominent FDA-endorsed CD19-targeted CAR-T cell products include Axicabtagene-ciloleucel (Axicel), Tisagenlecleucel (Tisacel), Lisocabtagenemaraleucel (Lisocel), and Brexucabtageneautoleucel (Brexucel). In the realm of BCMA-targeted CAR-T cells, the treatment boasts a notable complete response rate spanning from 73% to 98%. Regulatory approvals have been granted for the management of patients with relapsed and/or refractory multiple myeloma. Leading FDA-approved BCMA-targeted CAR-T cell products encompass Idecabtagenevicleucel (Idecel) and Ciltacabtageneautoleucel (Ciltacel). These CAR-T cell constructs fall under the classification of 2nd generation CARs, distinguished by their unique attributes in the Hinge region, Transmembrane region, and Co-stimulatory domain.(12)

The selection of co-stimulatory domains imparts distinctive dynamics to CAR-T cell therapies. Notably, the 4-1BB co-stimulatory domain is characterized by gradual expansion kinetics and prolonged persistence, in contrast to the CD28 co-stimulatory domain, which is recognized for its rapid expansion but relatively limited durability.(13)

1.4 Limitation of CAR-T cell therapy

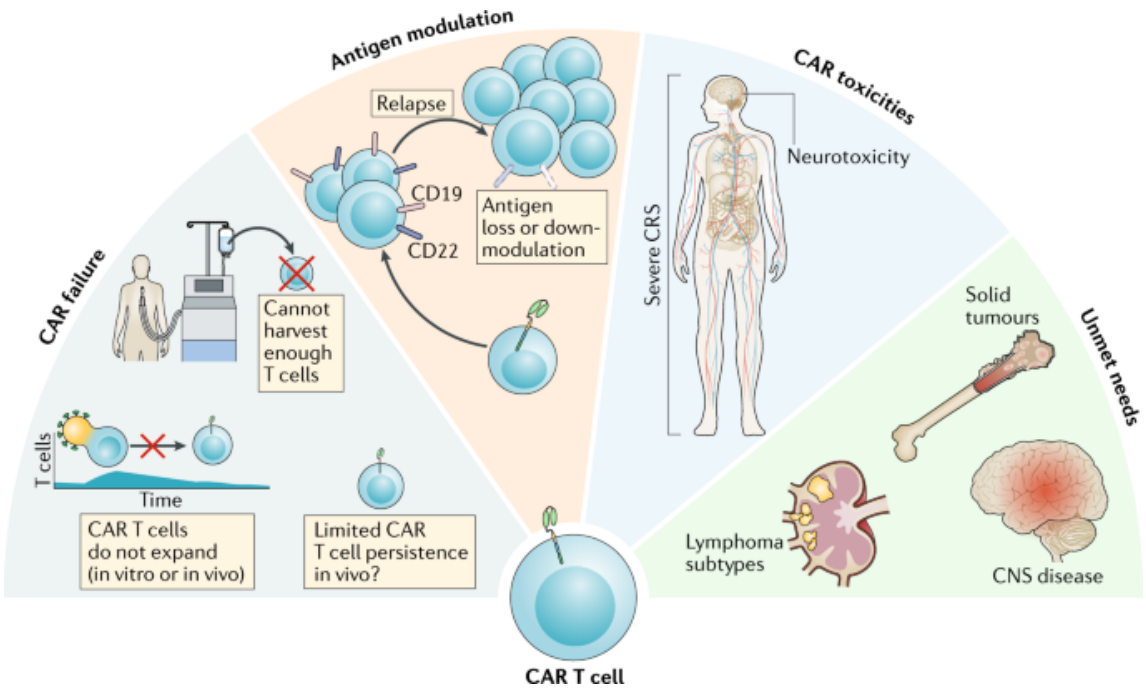

Figure 6: Limitations of CAR-T cell therapy (15)

While CAR-T cell therapy exhibits considerable promise, it is beset by a multitude of inherent limitations. These limitations encompass CAR failure, antigen modulation, CAR toxicities, and unfulfilled clinical needs. CAR failure entails scenarios in which CAR-T cells fail to exhibit adequate expansion or persistence within the in vivo environment, as well as insufficient T cell harvest from the patient. Antigen modulation, on the other hand, signifies the cancer cells' capacity to dynamically alter their antigen expression profiles, rendering the targeted antigens elusive for CAR-T cell recognition. Furthermore, CAR toxicities encompass the emergence of severe cytokine release syndrome (CRS) and neurotoxicity as adverse effects of therapy. The unmet clinical needs in this context extend to addressing challenging entities such as solid tumors, specific lymphoma subtypes, and central nervous system diseases. (14)

Research efforts aimed at surmounting these limitations are crucial to unleash the full potential of CAR-T cell therapy, paving the way for broader and more effective applications across diverse oncological and disease settings. Developing innovative

strategies to overcome these challenges will not only enhance the therapy's effectiveness but also expand its reach to benefit a larger spectrum of patients in need.(15)

Contemporary methodologies addressing the aforementioned limitations encompass the refinement of CAR constructs, mitigation of T cell dysfunctions, and the integration of chemical and external interventions. Modification of CAR constructs involves the augmentation of specificity, exemplified by the implementation of dual CARs targeting distinct tumor-related antigens. Tandem CARs, incorporating two or more scFvs in a linear assembly, akin to bispecific antibody platforms, have also emerged. An alternative strategy involves the design of universal CARs, where the CAR molecules split to the targeting domain, enabling binding to multiple undefined antigens. Additionally, Bispecific T cell Engager platforms have been developed, exhibiting versatility in targeting multiple antigens through combinatorial and sequential approaches, thereby redirecting T cell activity towards tumor cells. Further explorations include the engineering of T cells for the recognition of tumor cells through the induction of bystander T cell activation, facilitated by the transgenic expression of cytokines or ligands. Extensive investigations have been conducted on switch-controlled CARs, which govern activation to selectively eliminate tumors while incorporating inhibitory mechanisms, such as CAR-T cell suicide activation and regulatory pathways for co-stimulation. Despite notable successes in B lymphoblastic leukemia patients, a pervasive challenge is the limited sustained response of most patients to CAR T cells, predominantly attributable to T cell dysfunction. Chemical compounds have emerged as potential adjuncts to augment target antigen expression or enhance T cell activities, exerting synergistic effects on CAR T cell function.(16)

In the scope of our project, we are directing our investigative efforts toward ameliorating the limited persistence of CAR-T cells in vivo, with a particular emphasis on their application in treating solid tumors.

1.5 CAR-Enhancer

To tackle the obstacle of limited CAR-T cell persistence, studies have attempted to re-engineer CAR-T cells to knock out or knock in genes involved in T cell activation and exhaustion respectively, or engineer “switch receptors” on CAR-T cells that transform inhibitory signals into stimulatory signals. Although promising, these approaches require additional engineering of the CAR-T cell with some important disadvantages such as difficult design and operation, promoter silencing, and potential mutations caused by modification to deoxyribonucleic acid (DNA) that can exacerbate toxicities associated with treatment. An alternative strategy to improve CAR-T cell persistence is the supplementation of combinatorial cytokines such as IL2, as it’s known to lead to T cell proliferation and effector function. However, due to a lack of specificity of delivered cytokines, adverse effects are common. To overcome these issues, we developed an antigen-based CAR-Enhancer (CAR-E). (17–20)

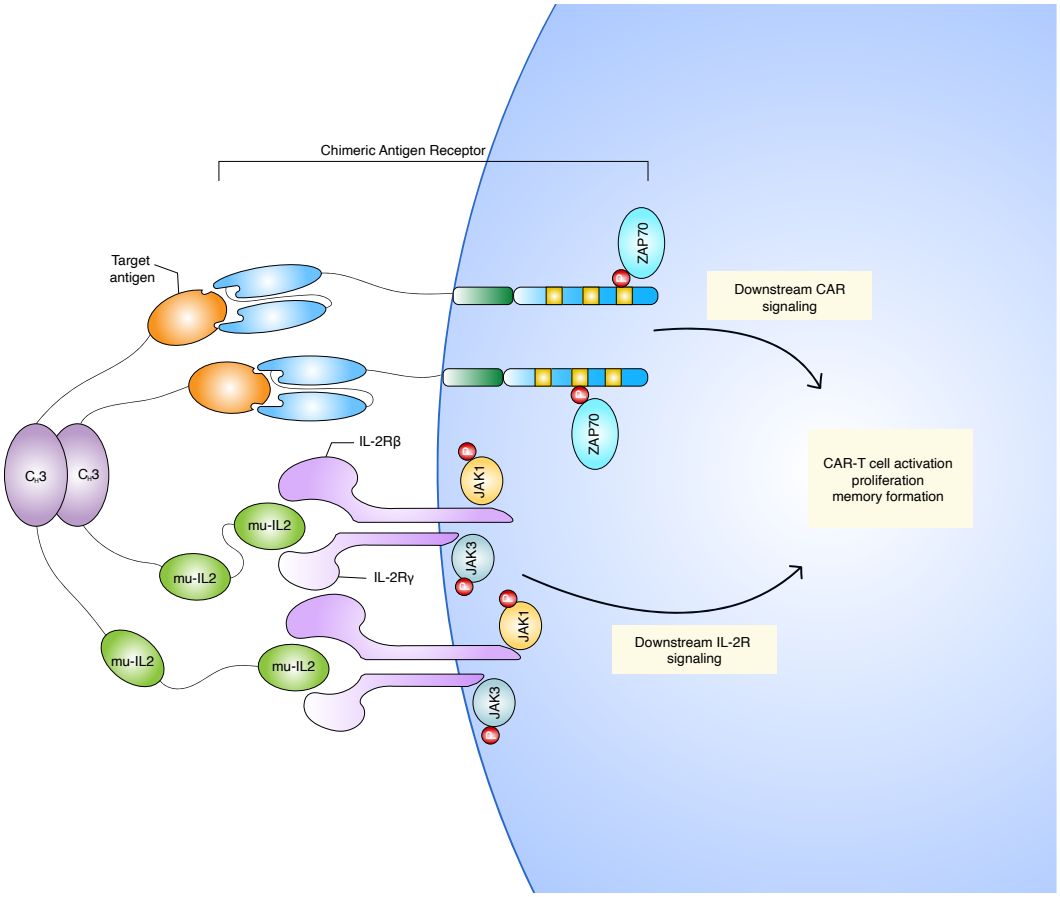

Figure 7: Structure of CAR-E

This enhancer contains the BCMA or CD19 antigen which can bind to the CAR-T cell and a mutated IL2, which has a lower affinity for the IL2 receptor. Thereby, the CAR-T cell is stimulated and activated leading to CAR-T cell expansion and tumor clearance without impacting endogenous immune cell populations. Furthermore, it is an off-the-shelf product and can be added as a treatment to the already approved CAR-T cells.

We hypothesize that the engineered CD19-CAR-E improves the efficacy of FDA-approved CAR-T cells. Upon CAR-E treatment, CAR-T cell therapies are more effective against solid tumors and lead to prolonged remissions through the generation of memory CAR-T cells. Our research endeavors revolve around the identification and characterization of optimal mutations within the IL2 molecule that engender reduced affinity. Additionally, our investigations aim to elucidate the differential treatment responses between Lisocel and Axicel. The precise mechanisms underpinning the augmentation of CAR-T cell function and CAR-E remain incompletely understood. Unraveling this mechanism could unlock a novel link between IL2 and CAR-T cells.

The initial phase in elucidating this entails the construction of therapeutically relevant CAR-Es. We propose that the ectodomain of the human CD19 protein can effectively target CD19 CAR-T cells. Additionally, we hypothesize that mutating the IL2 segment of CAR-E to possess minimal affinity to the IL2 receptor will significantly mitigate off-target effects.

The subsequent phase involves the production of CAR-E. We postulate that CAR-E can be recombinantly produced and purified in such a way that it is safe to use in mammalians.

The third stage aims to characterize the efficacy of CAR-E in vitro. We anticipate that CAR-E will induce heightened activation, proliferation, and cytotoxicity in CD19-CAR-T cells. To assess this, activation assays, proliferation assays, and killing assays will be conducted.

In the fourth stage, the evaluation encompasses the in vivo assessment of CAR-E impact. Our hypothesis posits that CAR-E will induce heightened CAR-T cell activity,

resulting in superior efficacy in clearing the Nalm6 and Raji tumor models compared to sole CAR-T cell therapy. Additionally, we postulate that the combined presence of CAR-T cells and CAR-E facilitates CAR-T cell expansion in the absence of cancer cells.

2 Methods and Materials

2.1 Protein Production

Protein production was achieved through the cellular secretion of proteins by HEK 293 cells. These HEK 293 cells were transfected using a plasmid containing genetic information for the secretion of the target protein. The transfected HEK 293 cells were cultivated in cell culture-treated plates with Dulbecco's Modified Eagle Medium (DMEM) containing 10% Fetal Bovine Serum (FBS), 1% Penicillin/Streptomycin, 1% non-essential amino acids (MEM NEAA), 1% Pyruvate, and maintained at a temperature of 37°C in an incubator. Upon reaching approximately 70% confluence, a puromycin selection process was initiated. The transfected plasmid included a puromycin resistance gene, enabling the removal of cells that did not produce high quantities of the desired protein through puromycin selection. After a 2-day period, the cells were detached using Trypsin and then distributed to the desired number of poly-L-lysine-coated plates. Poly-L-lysine coating facilitated cell adhesion to the plates. These plates were subsequently incubated at 37°C until they reached 100% confluence. Upon achieving full confluence, the culture medium was aspirated, the plates were rinsed with phosphate-buffered saline (PBS), and fresh medium was added. The new medium consisted of DMEM supplemented with 1% Penicillin/Streptomycin, 1% MEM NEAA, 1% Pyruvate, and 0.25% Bovine Serum Albumin (BSA), which promoted protein secretion by the cells. Culture medium harvests were performed at intervals of 3-4 days.

2.2 Protein Purification

Protein purification was accomplished using a two-step process involving Immobilized Metal Affinity Chromatography (IMAC) and Dialysis. After an adequate amount of media from protein-producing cells was collected, the purification using IMAC columns could start. The protein of interest has a polyhistidine tag incorporated and could therefore be selectively retained within the $NiSO_4$-loaded column. Subsequently, the protein was eluted through a high concentration of Imidazole, which

outcompetes the histidine tag and chelates with Nickel, thus eluting the protein. Elution fractions, containing 0.5 mM Ethylenediamine tetraacetic acid (EDTA), to prevent protein aggregation through chelation, were gathered, and protein concentrations were determined via the NanoDrop One Spectrophotometer. To collect the protein, fractions containing the highest protein content were combined. These combined fractions underwent dialysis using SnakeSkin Dialysis Tubing. The initial dialysis was conducted in a dialysis buffer composed of 150 mM NaCl, 50 mM 1-(2-hydroxyethyl)-1-piperazineethanesulfonic acid (HEPES), 0.5 mM EDTA, with a pH range of 7 to 8, and maintained at 4°C for a minimum of 3 hours. Subsequently, the buffer was exchanged for a dialysis buffer consisting of 150 mM NaCl, 50 mM HEPES, and a pH range of 7 to 8, also for at least 3 hours at 4°C. If necessary, the dialyzed protein was diluted to a concentration of 0.5-2 mg/ml with PBS. Glycerol was then added to achieve a final concentration of 5%, and the protein was sterile filtered. The protein underwent aliquoting, flash freezing, and storage at -20°C for preservation.

2.3 Quality Control

To ascertain the identity and purity of the synthesized protein a Sodium Dodecyl Sulfate Polyacrylamide Gel Electrophoresis (SDS-PAGE) was conducted. The gel used for SDS-PAGE was prepared as follows: A running gel comprising 10% SureCast acrylamide, SureCast Resolving Buffer, and distilled water was polymerized using 10% ammonium persulfate (APS) and 0.1% N, N, N’, N'-Tetramethylethylenediamine (TEMED). A thin layer of isopropanol was applied to ensure a uniform surface. The stacking gel was composed of 4% SureCast acrylamide, SureCast running buffer, and distilled water. It was cast using an appropriate well comb. The protein samples were mixed with NuPAGE LDS sample buffer. For the positive control, 1µL of dithiothreitol (DTT) was added to the sample and heated for 5 minutes at 95°C. Subsequently, the gel was placed in an electrophoresis chamber filled with SDS running buffer. The protein samples and a prestained ladder were loaded onto the gel, and electrophoresis was performed at 120 Volts for a duration sufficient to visualize all distinct protein bands. Following electrophoresis, the gel was removed from the chamber and stained with Coomassie Stain for 30 minutes. Subsequently,

the gel was destained using distilled water for 2 hours. Finally, the gel was imaged using a ChemiDoc Imaging System for further analysis and documentation.

2.4 CAR-T cell production

Human Peripheral Blood Mononuclear Cells (PBMCs) were thawed and introduced into a non-tissue culture-treated 6-well plate. These cells underwent a specific isolation procedure involving the addition of 500x α-human CD3 and 1000x α-human CD28, IL2, IL7, and IL15 to specifically target and separate T cells.

The subsequent day, media containing the virus derived from previously prepared plates holding gamma-retrovirus-producing cells was gathered and filtered using a 45 µm filter. In parallel, a 6-well plate coated with retronectin was treated by blocking it for 30 minutes at 37°C with a 2% BSA solution. The gathered PBMCs were resuspended in 6 mL of complete Roswell Park Memorial Institute (RPMI) media, including 10% FBS, 1% Penicillin/Streptomycin, 1% MEM NEAA, and 1% Pyruvate. The cytokines (IL2, IL7, IL15), CD3, and CD28 were introduced into the 6mL suspension thrice, and the cells were evenly distributed across the retronectin-coated plate. Among the wells, 2mL of viral media was added to 5 wells while 1 well was preserved as an untransduced control. Subsequently, the plate was subjected to centrifugation at 30°C, at 2000g for 1 hour, and then maintained at 37°C.

The subsequent day, transduced PBMCs were pelleted in the plate and 2 mL from each well were aspirated. In 5 wells, the aspirated volume was replaced with 2 mL of viral media, while 2 mL of complete RPMI was added to 1 well. Cytokines were supplemented in each well, followed by centrifugation at 30°C, at 2000g for 1 hour, and maintenance at 37°C.

The resulting CAR-T cells, Axicel and Lisocel, were transferred to cell culture-treated flasks and maintained at a concentration of 1 million cells/mL in complete RPMI media, supplemented with 1000x concentrations of IL2, IL7, and IL15.

To determine transduction efficiency, flow cytometry was employed. The cells were stained with α-human CD19 antibodies for analysis.

2.5 In vitro assays

2.5.1 Binding assay – Determination of EC50

To ascertain the EC50, the median effective concentration, a serial dilution of CAR-E must be prepared, encompassing concentrations of 100 nM, 10 nM, 5 nM, 3 nM, 1 nM, 0.5 nM, 0.1 nM, 0.01 nM, 0.001 nM, and 0.0001 nM. Lisocel and Axicel are each seeded into individual wells of a 96-well plate at a cellular density of 10,000 cells per well. Subsequently, the cells are centrifuged at 600g for 3 minutes, and the supernatant is removed. Each well is then suspended in 50 µL of the aforementioned prepared serial dilution. The plate is incubated for 20 minutes at 4°C. Following incubation, the plate is subjected to washing with 150 µL of FACS buffer, consisting of 1% BSA, per well. Subsequently, the cells are centrifuged at 600g for 3 minutes, the supernatant is aspirated, and the cells are resuspended in 50 µL of a secondary stain, an α-DYKDDDDK (FLAG) tag, labeled with Alexa Fluor 647. The α-FLAG tag specifically binds to the CAR-E due to its FLAG tag. Incubation with the secondary stain occurs for 20 minutes at 4°C. Post-incubation, further washing of the cells with FACS buffer is performed. Following this, cells are once again centrifuged at 600g for 3 minutes and resuspended in 200 µL/well of FACS buffer. The fluorescence intensity is then quantified utilizing flow cytometry on the BD FACSCanto II system. The resulting flow cytometry data underwent analysis using FlowJo software, and graphical representations were generated using Prism GraphPad.

2.5.2 CAR-T cell activation assays

To ascertain the activation induced by CAR-E on CAR-T cells, various activation assays are conducted. These assays comprise assessments for CD69 and pSTAT5 activation, alongside an Enzyme-Linked Immunosorbent Assay (ELISA) aimed at delineating the cytokine profile after activation of the CAR-T cells.

2.5.2.1 CD69 activation assay

CAR-T cells are dispensed into a 96-well plate at a density of 100,000 cells in 180 µL of complete RPMI per well. A serial dilution of CAR-E is prepared, encompassing concentrations of 1000 nM, 100 nM, 10 nM, 1 nM, 0.1 nM, and 0.01 nM. Each concentration is executed in triplicates. Subsequently, 20 µL per well of the serially diluted CAR-E is introduced to the cell-containing plate. The plate undergoes a 2-hour incubation period at 37°C. Post-incubation, cells are centrifuged at 600g for 3 minutes. The resultant supernatant is discarded. This washing step replicates the anticipated behavior of CAR-E in the patient's system, considering its notably short half-life. For further analysis, cells are resuspended in 200 µL of complete RPMI per well and incubated for 24 hours at 37°C. Following this incubation period, the cells are pelleted, and the resulting supernatant is collected and stored at -20°C for the subsequent determination of the cytokine profile. Afterwards, a staining solution consisting of 100nM of CD19-minibody is prepared to quantify the presence of CAR-T cells. Cells are exposed to 50 µL per well of this stain and incubated for 20 minutes at 4°C. The cells are washed using FACS buffer and a secondary stain comprising α-FLAG tag Alexa Fluor 647, to detect the bound CD19-minibody, and α-CD69 PE is prepared. Each well receives 50 µL of this stain and incubates for 20 minutes at 4°C. Following this, another washing step with 150 µL of FACS buffer per well is performed. The fluorescence intensity of the assay is quantified by flow cytometry using BD FACSCanto II system. The resulting flow cytometry data underwent analysis using FlowJo software, and graphical representations were generated using Prism GraphPad.

2.5.2.2 Phosphorylated STAT5 (pSTAT5) activation assay

CAR-T cells were dispensed into a 96-well plate at a density of 100,000 cells in 180 µL of complete RPMI per well. A series of dilutions of CAR-E were prepared, spanning concentrations of 100 nM, 10 nM, 1 nM, 0.1 nM, 0.01 nM, and 0.001 nM. Each concentration was replicated in triplicate. Subsequently, 20 µL of the serially diluted CAR-E was added to the plate containing the cells. For the 30-minute time point, the plate underwent a 30-minute incubation period at 37°C. Following this, the cells were fixed using 1.5% Formaldehyde, permeabilized using 100% ice-cold Methanol,

washed with FACS buffer, and stained for phosphorylated STAT5. The fluorescence intensity was quantified by flow cytometry using BD FACSCanto II system. The resulting flow cytometry data underwent analysis using FlowJo software, and graphical representations were generated using Prism GraphPad. For the 24-hour timepoint, the plate underwent a 2-hour incubation period at 37°C. After incubation, cells were centrifuged at 600g for 3 minutes, and the resulting supernatant was discarded. This washing step aimed to simulate the expected behavior of CAR-E in the patient's system, considering its notably short half-life. For further analysis, cells were resuspended in 200 µL of complete RPMI per well and incubated for 24 hours at 37°C. Following the incubation period, the steps described earlier were repeated to quantify the fluorescence intensity of phosphorylated STAT5.

2.5.2.3 ELISA

To assess the cytokine profile of activated CAR-T cells, an ELISA was conducted. Initially, a 96-well plate was coated overnight at 4°C with specific capture antibodies against interferon (IFN) γ, or tumor necrosis factor (TNF) α. Subsequently, the plate underwent washing thrice using a wash buffer comprising 0.1% Tween-20 in PBS. Following this, the plate was blocked with 4% BSA and incubated at room temperature with agitation for 1 hour. Post-incubation, the plate was washed three times. The collected media from the CD69 activation assay was diluted at a ratio of 1:10 for IFNγ, and 1:5 for TNFα. Standard solutions containing varying concentrations of IFNγ, or TNFα (1000 pg/mL, 500 pg/mL, 250 pg/mL, 125 pg/mL, 62.5 pg/mL, 31.3 pg/mL, 15.6 pg/mL, 7.8 pg/mL, and 0 pg/mL) were added to each plate along with the diluted media. An additional incubation of 2 hours at room temperature ensued. After this incubation, the plate underwent another round of washing (three times). A biotin-labeled detection antibody specific to either IFNγ, or TNFα was introduced and allowed to incubate for 1 hour at room temperature with agitation. Following this incubation, the plate was washed three times. Avidin-horseradish peroxidase (HRP) was then added to the plate and incubated for 30 minutes at room temperature, followed by three washes. To initiate an enzymatic colorimetric reaction, 3,3',5,5'-Tetramethylbenizidine (TMB) substrate was added to the plate. The color reaction was allowed to proceed, and upon completion, it was terminated using H_2SO_4. The

optical density resulting from the color change was measured at 450 nm using SpectraMax M5. The resulting optical density was first analyzed using Microsoft Excel, and graphical representations were generated using Prism GraphPad.

2.5.3 Proliferation assay

PBMCs were exposed to ionizing radiation at a dose of 50 Gray (Gy) and subsequently combined with CAR-T cells at a ratio of 50:1 (PBMCs: CAR-T cells). This cell mixture was then cultured for three days in complete RPMI medium supplemented with 50 ng/mL of OKT3 at a temperature of 37°C. Following this resting period, the ratio of PBMCs to CAR-T cells was quantified by flow cytometry using the BD FACSCanto II system. 3600 CAR-T were seeded into a flat-bottom, non-treated-tissue-culture 96-well plate in 180 µL. Subsequently, these CAR-T cells were exposed to 20 µL of the designated treatment with increasing dosage for an additional four days at 37°C. Following this incubation period, the number of CAR-T cells was assessed using flow cytometry for quantification. The resulting flow cytometry data underwent analysis using FlowJo software, and graphical representations were generated using Prism GraphPad.

2.5.4 Killing assays

Green fluorescent protein (GFP) -expressing Nalm6 cells and CAR-T cells were seeded at varying ratios of 1:1, 1:2, 1:5, and 1:10 (Effector: Target) in a flat-bottom, nontreated-tissue-culture 96-well plate. Subsequently, these co-cultures were exposed to increasing doses of treatment and maintained at 37 °C. Measurements were taken at two distinct time points: 24 hours and 48 hours post-treatment. The quantification of viable Nalm6 cells was conducted via flow cytometry using the BD FACSCanto II system. The resulting flow cytometry data underwent analysis using FlowJo software, and graphical representations were generated using Prism GraphPad.

2.6 In vivo experiments

2.6.1 Mice methods

The experimental mice, procured from Jackson Laboratory, were housed in the Animal Research Facility operated by the Dana-Farber Cancer Institute and another one operated by the Boston Children's Hospital. The specific strain used was NSG-MHC I/II DKO, which has a severe immunocompromised state, enabling the receipt of CAR-T cell injections. Trained facility personnel vigilantly monitored the mice. Biweekly weight assessments to ensure their well-being were conducted. In cases where weight reduction was observed, interventions such as HydroGel supplementation and increased food provision were implemented. If a mouse experienced a 20% decline in body weight, humane euthanasia procedures were enacted. Tumor cell lines, namely Nalm6 and Raji, were utilized for injections. Nalm6 cells were administered intravenously, representing a liquid tumor model anticipated to be more susceptible to CAR-T cell clearance. Conversely, Raji cells were subcutaneously injected, serving as a solid tumor model, presenting a greater challenge for CAR-T cell clearance. CAR-T cells were delivered via intravenous injections. During intravenous administrations, mice were anesthetized using Isoflurane to ensure comfort and minimize distress. The treatment regimen involved biweekly dosing of CAR-E at 8 mg/kg, administered without anesthesia using insulin syringes.

2.6.2 Bio-Luminescent Imaging (BLI)

The Nalm6 and Raji cells were both characterized by their expression of Luciferase. Intraperitoneal injections of D-Luciferin were administered to enable BLI. Mice were anesthetized with isoflurane during the imaging procedure. The acquired BLI images were subjected to analysis utilizing Aura software from Spectral Instrument Imaging. Luminescence levels were evaluated in images captured following a 5-minute exposure to ensure maximal signal detection and visibility.

2.6.3 Endpoint analysis

In instances where an experimental endpoint was reached or if the mouse's welfare was deemed concerning, euthanasia was performed by inducing a CO_2 overdose followed by cervical dislocation, ensuring a swift and humane process. Subsequently, the mice underwent dissection procedures to obtain organs of interest. Immunological organs, notably the spleen and bone marrow, were processed by immersion in a solution composed of 1/3 complete RPMI media and 2/3 PBS. The spleen was gently crushed, and the bone marrow was extracted using a sterile insulin syringe. Solid organs were submerged in 3 mL of RPMI/PBS solution and further dissected into smaller fragments using scissors. After this, the organ pieces were incubated at 37°C for 30 minutes after exposure to 100 µL of Collagenase. Following the incubation period, the obtained samples were filtered using 100 nm filters and subsequently treated with ammonium-chloride-potassium (ACK) Lysis buffer for approximately 1 minute to induce lysis of red blood cells. The samples were then washed with FACS buffer and either prepared for flow cytometric analysis or preserved by freezing for subsequent analysis.

2.6.4 Flow cytometric analysis

The samples were subjected to incubation in a primary stain solution comprising a CD19 minibody, specifically targeting CD19. Subsequently, a secondary stain solution was formulated, incorporating specific antibodies: anti-CD45-PacificBlue and anti-FLAG-AlexaFluor647. These antibody solutions were suitably diluted in FACS buffer and then incubated with the samples for 20 minutes at a temperature of 4°C. Following the incubation period, the samples were thoroughly washed and suspended in FACS buffer. Depending on the specific requirements of the experiment, the samples were analyzed using the SP6800 Sony Spectral Analyser, capable of accommodating a broader spectrum of fluorophores.

2.7 Materials

Table 1:Manufacturer and Catalog numbers of Materials

Material	Manufacturer	Catalog number
APS	Santa Cruz Biotechnology	SC-202946A
anti-CD45-PacificBlue	BioLegend	304029
Anti-CD69-PE	BioLegend	310909
Anti-FLAG-AlexaFluor647	BioLegend	637316
Anti-hCD3-OKT3	Bioxcell	BE0001-2-R005MG
Anti-pSTAT5-APC	BioLegend	936906
BSA	Cell Signaling Technology	9998S
CD28	BioLegend	302902
Collagenase	StemCell Technologies	07912
DTT	Thermo Fisher Scientific	15508-013
DMEM	Thermo Fisher Scientific	11965-118
EDTA	Life Technologies	17892
ELISA MAX Deluxe Set Human IFN-γ	BioLegend	430104
ELISA MAX Standard Set Human TNF-α	BioLegend	430201
FBS	Thermo Fisher Scientific	26140-079
Formaldehyde	Santa Cruz Biotechnology	SC-203049
Glycerol	Santa Cruz Biotechnology	SC-29095A
H_2SO_4	Aldon Corp SE	SS1125-500ML
HEPES	Fisher BioReagent	BP3101
HiTrap IMAC FF	Sigma Aldrich	GE17-0921-04
IL15	Miltenyi Biotec	130-093-955
IL2	Cell Signaling Technology	8907SF
IL7	Sigma Aldrich	I5896
Insulin syringes	Amerisource Bergen	2438158
Methanol	Thermo Fisher Scientific	A4524

TEMED	Santa Cruz Biotechnolgy	SC-29111
NaCl	Fisher BioReagent	BP3581
MEM NEAA	Thermo Fisher Scientific	11140-050
NSG-MHC I/II DKO	The Jackson Laboratory	025216
NuPAGE LDS sample buffer	Thermo Fisher Scientific	NP0007
NuPAGE SureCast running buffer	Life Technologies	NP0002-02
PBS	Thermo Fisher Scientific	MT21040CV
Penicillin/Streptomycin	Gemini Bioproducts LIc	400-109
Poly-L-lysine	Sigma-Aldrich	P8920-100ML
Puromycin	Fisher BioReagent	BP2956100
Retronectin	Takara Bio	T100B
RPMI	Thermo Fisher Scientific	11875-119
Sodium pyruvate	Thermo Fisher Scientific	11360070
SureCast acrylamide 40%	Life Technologies	HC2040
SureCast Resolving Buffer	Life Technologies	HC2215
TMB Substrate Set	BioLegend	421101
Trypsin 0.25% EDTA	Thermo Fisher Scientific	25200-114
Tween-20	Santa Cruz Biotechnology	SC-29113

3 Results

3.1 In vitro characterization of the CAR-E

3.1.1 CAR-E constructs

The initiation of the project required the generation of four specific constructs. These constructs are CD19-CH3-mutIL2, CD19-CH2-CH3-mutIL2, CD19-CH3 targeting CD19-CAR-T cells, and BCMA-CH3-mutIL2 targeting BCMA-CAR-T cells. The IL2 domain, integral to these constructs, comprises two copies of the original cytokine, each carrying three mutations. The first mutation, H16A, decreases the affinity towards the IL2-Receptor-β (IL2-R-β) by approximately threefold. The second mutation, F42A, significantly diminishes the affinity towards the IL2-Receptor-α (IL2-R-α) by about 100-fold. The last mutation, Y45A, also plays a role in modulating receptor affinity. The initial mutation plays a pivotal role in transducing the signal, thereby necessitating the preservation of a certain level of IL2 activity through the careful modulation of its affinity. (20) Conversely, the alpha subunit predominantly functions as a signaling anchor, a function that is now assumed by the CAR. Incorporating the CH3 domain of the IgG1 antibody serves a dual purpose: enhancing signaling capability and substantially reducing the protein's half-life, facilitating rapid clearance from circulation. Unlike full-size antibodies (CH2-CH3), which endure longer in circulation through recognition and recycling via FcRn in the kidneys, the CH3 domain in CD19-CH3-mutIL2 aims to extend IL-2 exposure to CAR-T cells by stimulating pulsatile rather than sustained signaling. Prolonged signaling might potentially induce CAR-T cell exhaustion or terminal differentiation.

Confirmation of the protein expression involved conducting SDS-PAGE on a polyacrylamide gel. The CH3 and CH2-CH3 domains respectively, form stable dimers, which could be denatured by heating and the addition of DTT before loading samples into the gel.

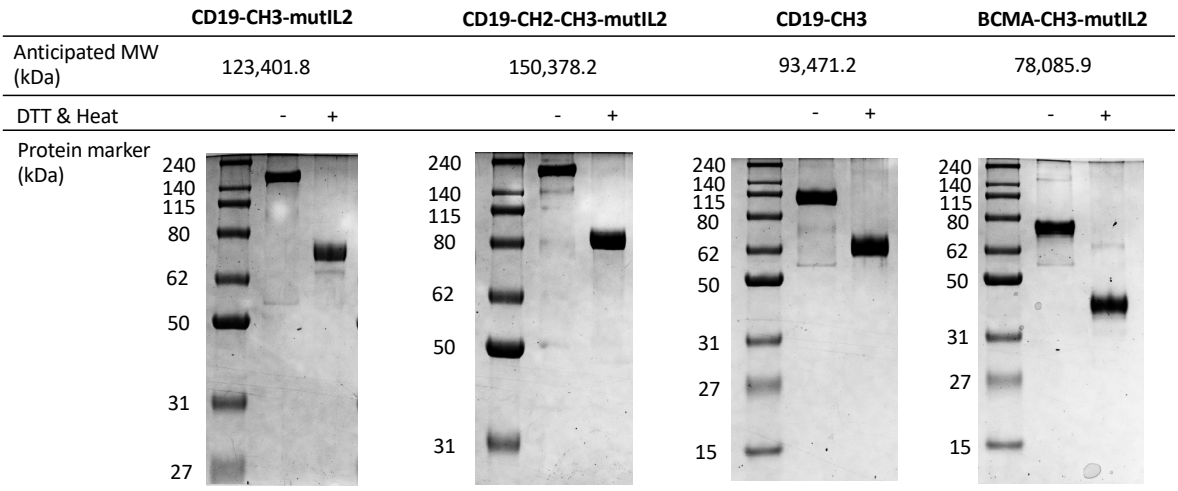

Figure 8: CAR-E constructs on SDS-PAGE

Upon analysis of **Figure 8**, the gel lanes corresponding to each construct manifest the presence of dimers without the addition of DTT and heat, while monomers are observed with DTT and heat treatment. The molecular weights of these entities are as follows:

- CD19-CH3-mutIL2 demonstrates a dimeric size of 123,401.8 kDa and a monomeric size of 61,700.9 kDa.
- CD19-CH2-CH3-mutIL2 displays a dimeric size of 150,378.2 kDa, with its monomer weighing 75,189.1 kDa.
- CD19-CH3 exhibits a dimeric size of 93,471.2 kDa, while its monomer weighs 46,735.8 kDa.
- BCMA-CH3-mutIL2 showcases a dimeric weight of 78,085.9 kDa and a monomeric weight of 39,043 kDa.

Moreover, **Figure 8** provides a visual representation indicating the purity of the aforementioned constructs.

3.1.2 Assessment of binding efficacy of the CAR-E

To evaluate the functionality of the CAR-E, the initial step involved the assessment of its binding efficacy. Axicel and Lisocel were exposed to varying concentrations of the CAR-E constructs. Subsequently, flow cytometry analysis was conducted to ascertain the EC50, representing the concentration at which half-maximal effective binding occurred.

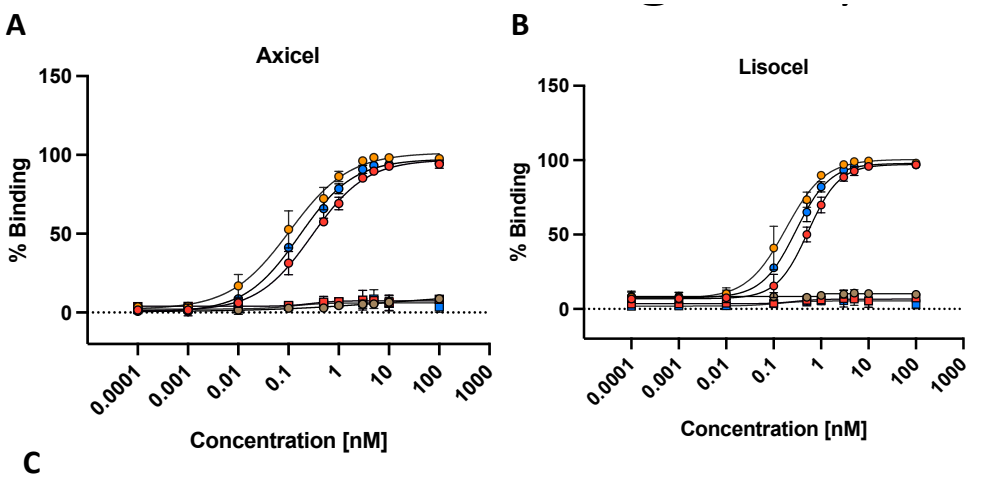

C

EC50		
Treatment	CAR-T cell	
	Axicel	*Lisocel*
CD19-CH3-mutIL2	0.2942	0.5349
CD19-CH3	0.1058	0.1812
CD19-CH2-CH3-mutIL2	0.1653	0.2962

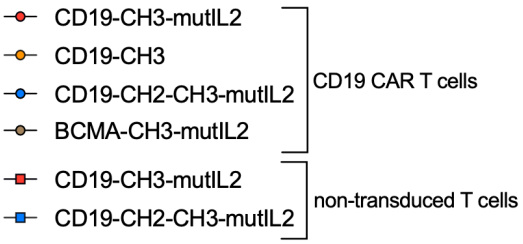

*Figure 9: illustrates the specific binding characteristics of CAR-E to Axicel and Lisocel **A)** presents the binding profiles of CD19-CH3-mutIL2, CD19-CH3, CD19-CH2-CH3, and BCMA-CH3-mutIL2 on Axicel and non-transduced T cells **B)** displays binding patterns of CD19-CH3-mutIL2, CD19-CH3, CD19-CH2-CH3, and BCMA-CH3-mutIL2 on Lisocel and non-transduced T cells **C)** provides a quantitative representation of the EC50 values for CD19-CH3-mutIL2, CD19-CH3, and CD19-CH2-CH3-mutIL2 on both Axicel and Lisocel, elucidating the nuances of binding affinity between the CAR-E constructs and the respective target cells.*

Figure 9A) illustrates the binding profiles observed on Axicel and non-transduced T cells. Notably, CD19-CH3-mutIL2, CD19-CH3, and CD19-CH2-CH3-mutIL2 exhibit analogous binding behavior. Their respective EC50 values are 0.2942 for CD19-CH3-mutIL2, 0.1058 for CD19-CH3, and 0.1653 for CD19-CH2-CH3-mutIL2, as depicted in **Figure 9C)**. BCMA-CH3-mutIL2 fails to bind to Axicel, suggesting a marked reduction in the affinity of the IL2 domain. Furthermore, both CD19-CH3-mutIL2 and CD19-CH2-CH3-mutIL2 do not demonstrate binding to non-transduced T cells. **Figure 9B)** showcases the binding curves observed on Lisocel and non-transduced T cells. Similar trends are evident compared to **Figure 9A)**. The calculated EC50 values are as follows: CD19-CH3-mutIL2 at 0.5349, CD19-CH3 at 0.1812, and CD19-CH2-CH3-mutIL2 at 0.2962. This suggests a generally higher EC50 for Lisocel compared to Axicel, indicating that the CAR-E exhibits a greater binding affinity towards Axicel.

3.1.3 Assessment of activation efficacy of the CAR-E

To further evaluate the functional capacity of the CAR-E, its activation potential was investigated. The CAR-E was incubated with varying concentrations separately with Axicel, Lisocel, or non-transduced T cells. Subsequently, assessments of pSTAT5 levels at 30 minutes and 24 hours, along with CD69 expression at 24 hours, were conducted. After 24 hours of incubation, the serum of the cells was collected and the cytokine profile was determined, focusing on IFNγ, and TNFα.

The pSTAT5 assays serve to gauge the activation status of the IL2 receptor. Activation of the IL2 receptor triggers the JAK-STAT pathway, culminating in the phosphorylation of STAT5.(21) Conversely, the CD69 assay is employed to monitor the activation of CAR-T cells, as CD69 undergoes upregulation following cellular activation.(22) Activated CAR-T cells exhibit a cytokine secretion profile characterized by the release of IFNγ and TNFα. It is noteworthy that the secretion of IFNγ surpasses that of TNFα.(23)

3.1.3.1 Activation on Axicel

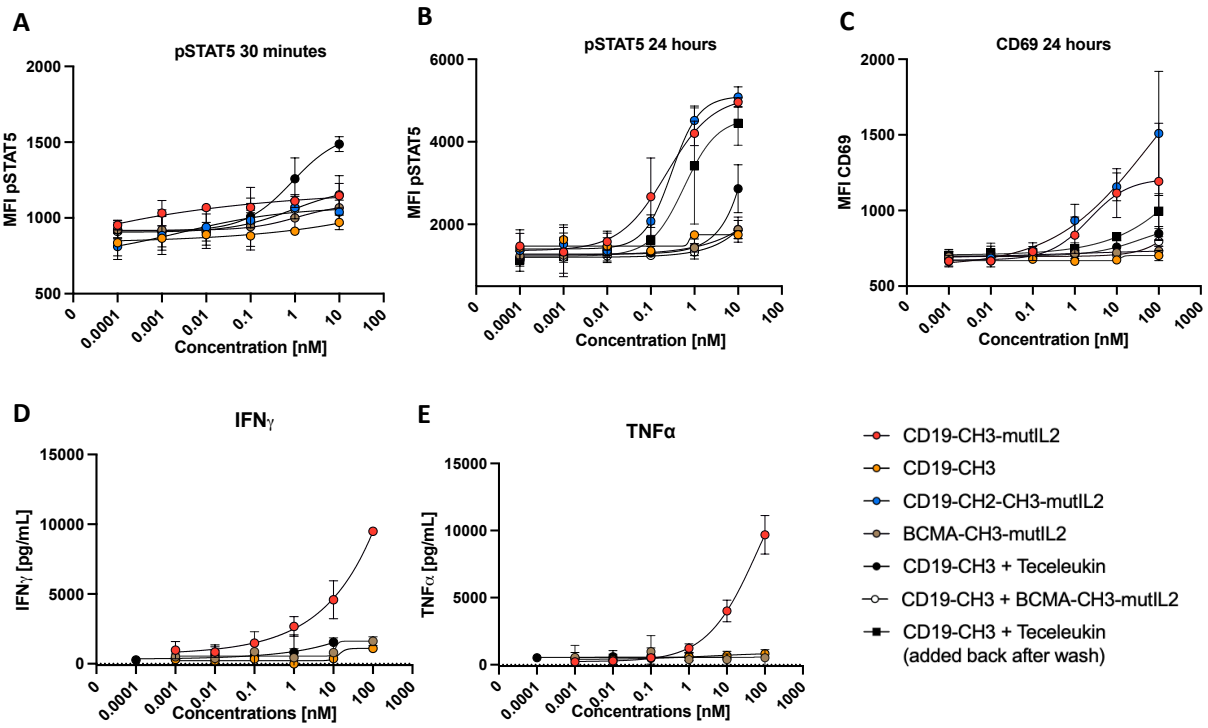

*Figure 10: Activation profile of Axicel **A)** delineates the Mean Fluorescence Intensity (MFI) of pSTAT5 after 30 minutes of incubation, providing insight into the early IL2 downstream activation **B)** extends the analysis to 24 hours of incubation, presenting the MFI of pSTAT5 **C)** illustrates the MFI of CD69 expression after 24 hours of incubation, offering a comprehensive view of CAR-T cell activation dynamics **D)** presents IFNγ secretion in pg/mL after 24 hours of incubation **E)** shows TNFα secretion in pg/mL after 24 hours incubation*

Figure 10 presents the activation assays on Axicel. **Figure 10A)** presents the pSTAT5 levels at 30 minutes in MFI. Teceleukin (IL2) demonstrates a direct correlation between increasing concentrations and elevated pSTAT5 levels. Notably, CD19-CH3 exhibits no activation due to its absence of the IL2 domain. Similarly, CD19-CH3-mutIL2, CD19-CH2-CH3-mutIL2, and BCMA-CH3-mutIL2 manifest no significant activation. Contrarily, after 24 hours (**Figure 10B)**), a distinct change in pSTAT5 levels is observed. CD19-CH3-mutIL2 and CD19-CH2-CH3-mutIL2 exhibit the highest activation among all conditions, surpassing even Teceleukin, which was reintroduced after the wash step. Notably, CD19-CH3 and BCMA-CH3-mutIL2 demonstrate negligible activation, highlighting the indispensability of the IL2 do-

main's association with the CD19-CH3 domain. BCMA-CH3-mutIL2 alone demonstrates activation levels akin to CD19-CH3. Furthermore, a marginal activation is observed with combined CD19-CH3 and Teceleukin at higher concentrations. **Figure 10C)** displays the CD69 assay results after 24 hours. CD19-CH2-CH3-mutIL2 exhibits the highest activation, closely followed by CD19-CH3-mutIL2. Subsequently, CD19-CH3 and Teceleukin, reintroduced post-wash, demonstrate moderate activation. Conversely, all other control conditions exhibit minimal activation. In summary, a dose-dependent activation pattern of the CAR-E is discernible from these observations. **Figure 10D) and E)** show the cytokine secretion of Axicel. Both IFNγ and TNFα are only secreted by CD19-CH3-mutIL2.

3.1.3.2 Activation on Lisocel

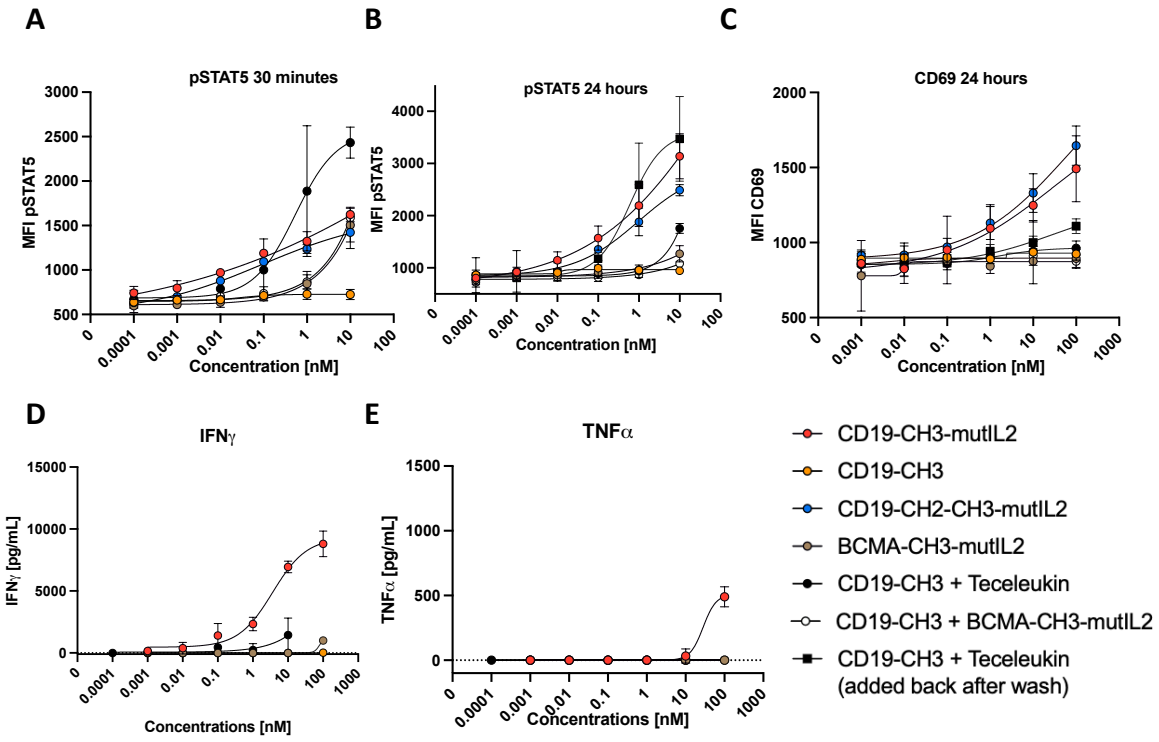

*Figure 11: Activation profile of Lisocel **A)** delineates the MFI of pSTAT5 after 30 minutes of incubation, providing insight into the early IL2 downstream activation **B)** extends the analysis to 24 hours of incubation, presenting the MFI of pSTAT5 **C)** illustrates the MFI of CD69 expression after 24 hours of incubation, offering a comprehensive view of CAR-T cell activation dynamics **D)** presents IFNγ secretion in pg/mL after 24 hours of incubation **E)** shows TNFα secretion in pg/mL after 24 hours incubation*

Figure 11 depicts the activation assays performed on Lisocel. In **Figure 11A)**, the pSTAT5 levels after 30 minutes exhibit Teceleukin displaying the highest activation of pSTAT5, while CD19-CH3 presents no discernible pSTAT5 levels. CD19-CH3-mutIL2, CD19-CH2-CH3-mutIL2, and other conditions demonstrate moderate activation. In **Figure 11B)**, showcasing pSTAT5 levels after 24 hours, the most significant activation is observed in CD19-CH3 with Teceleukin reintroduced post-wash, closely followed by CD19-CH3-mutIL2 and CD19-CH2-CH3-mutIL2. CD19-CH3 with Teceleukin exhibits minimal activation, whereas all other conditions display no activation. **Figure 11C)** exhibits the CD69 activation assay results. CD19-CH2-CH3-mutIL2 shows the highest activation, followed by CD19-CH3-mutIL2. CD19-CH3 and Teceleukin, reintroduced post-wash, display minimal activation, while all other conditions exhibit no activation. **Figure 11D) and E)** show the cytokine secretion of Lisocel. Both IFNγ and TNFα are only secreted by CD19-CH3-mutIL2. Although IFNγ is secreted at a higher level than TNFα.

Overall, the results closely resemble those in **Figure 10**. Notably, a discrepancy is evident between **Figure 11B)** and **Figure 10B)**, where Teceleukin demonstrates the highest activation for Lisocel, a pattern not observed for Axicel. Furthermore, the secretion of TNFα in **Figure 10E)** and **Figure 11E)** differs. Axicel secretes TNFα more than Lisocel.

3.1.3.3 Activation on non-transduced T cells

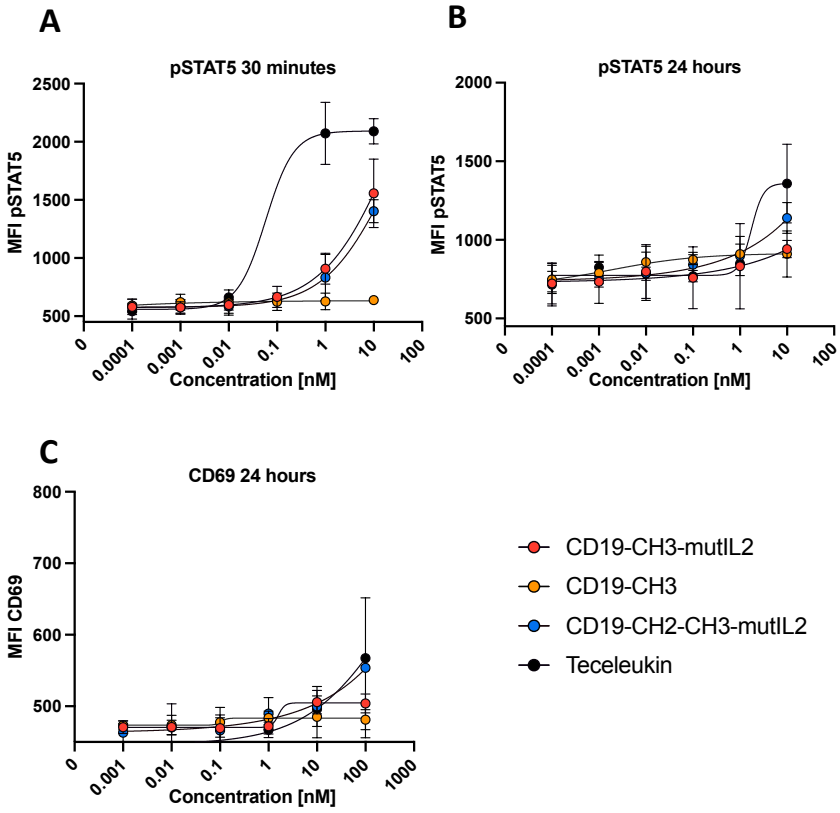

*Figure 12: Activation profile on non-transduced T cells **A)** presents the MFI of pSTAT5 after 30 minutes of incubation **B)** illustrates the MFI of pSTAT5 after 24 hours completing the picture of IL2 downstream activation **C)** delineates the MFI of CD69 after 24 hours of incubation, presenting the downstream activation of CAR-T cells*

Figure 12 illustrates the activation assays conducted on non-transduced T cells. In **Figure 12A)**, the pSTAT5 levels after 30 minutes exhibit Teceleukin inducing the highest activation, whereas CD19-CH3 shows no discernible activation. CD19-CH3-mutIL2 and CD19-CH2-CH3-mutIL2 demonstrate moderate activation, particularly noticeable at higher concentrations. This suggests that in the presence of a high concentration of CAR-E, the IL2 domain can bind to T cells despite its low affinity. **Figure 12B)** displays the pSTAT5 activation after 24 hours, revealing no substantial activation. In **Figure 12C)**, assessing CD69 activation, no significant activation is observed. These observations collectively suggest that the off-target effect of the

CAR-E is moderate after 30 minutes; however, after 24 hours, this effect diminishes, becoming imperceptible.

3.1.4 Assessment of proliferation efficacy

To assess the potential of CAR-E in augmenting the proliferation of CAR-T cells, a proliferation assay was conducted. CAR-T cells were incubated with irradiated PBMCs along with OKT3 for a duration of 3 days. Subsequently, the cells were exposed to varying concentrations of CAR-E for an additional 4 days. The quantification of CAR-T cell numbers was performed using flow cytometry.

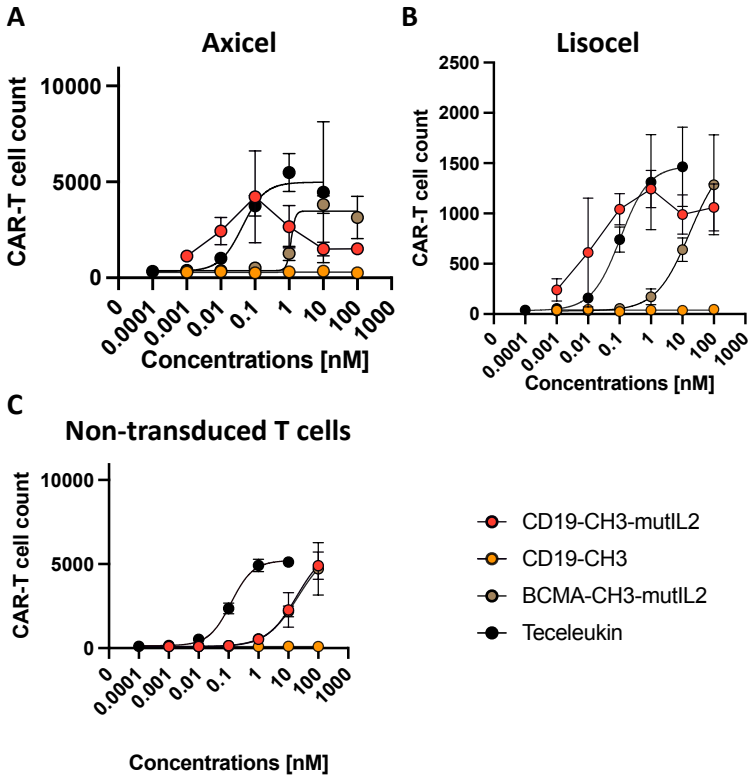

*Figure 13: Proliferation efficacy of CAR-T cells induced by CAR-E constructs **A)** depicts quantitative representation of cell counts for Axicel following incubation with CAR-E constructs **B)** illustrates the cell count dynamics of Lisocel upon exposure to CAR-E constructs **C)** shows the cell count of non-transduced T cells induced by the incubation with the CAR-E constructs*

In **Figure 13A)**, the proliferation of Axicel is depicted. CD19-CH3-mutIL2 induces proliferation up to a concentration of 0.1 nM, beyond which a decline in CAR-T cell

count is observed. This phenomenon may be attributed to potential overstimulation, given the elevated concentrations employed and the protracted incubation period of 4 days. This circumstance culminates in the subsequent diminution of CAR-T cell numbers. Conversely, BCMA-CH3-mutIL2 induces proliferation just at high concentrations. Teceleukin induces the proliferation of CAR-T cells without encountering a decline in cell numbers. Notably, CD19-CH3 does not induce proliferation. **Figure 13B)** illustrates the proliferation of Lisocel, revealing a comparable pattern to **Figure 13A)**. CD19-CH3-mutIL2 exhibits a decline after reaching 1 nM. Control groups show consistent results. In **Figure 13C)**, the proliferation of non-transduced T cells is presented to evaluate off-target effects. The off-target effect is minimal, with T cells initiating proliferation only at exceptionally high concentrations. This suggests a low likelihood of off-target effects associated with the tested conditions. In summary, it can be deduced that CAR-E elicits heightened proliferation of CAR-T cells, while demonstrating negligible impact on non-transduced T cells.

3.1.5 Assessment of killing efficacy of the CAR-E

To assess the cytotoxic efficacy and inhibitory potential of CAR-E on CAR-T cells, a killing assay was executed. In this assay, CAR-T cells and Nalm6 cells were co-incubated at varying effector-to-target (E: T) ratios for durations of 24 and 48 hours, without intervening wash steps. The objective of this assay is twofold: firstly, to determine if the treatment impedes the receptor, and secondly, to establish evidence supporting the CAR-E's capacity to enhance cytotoxicity.

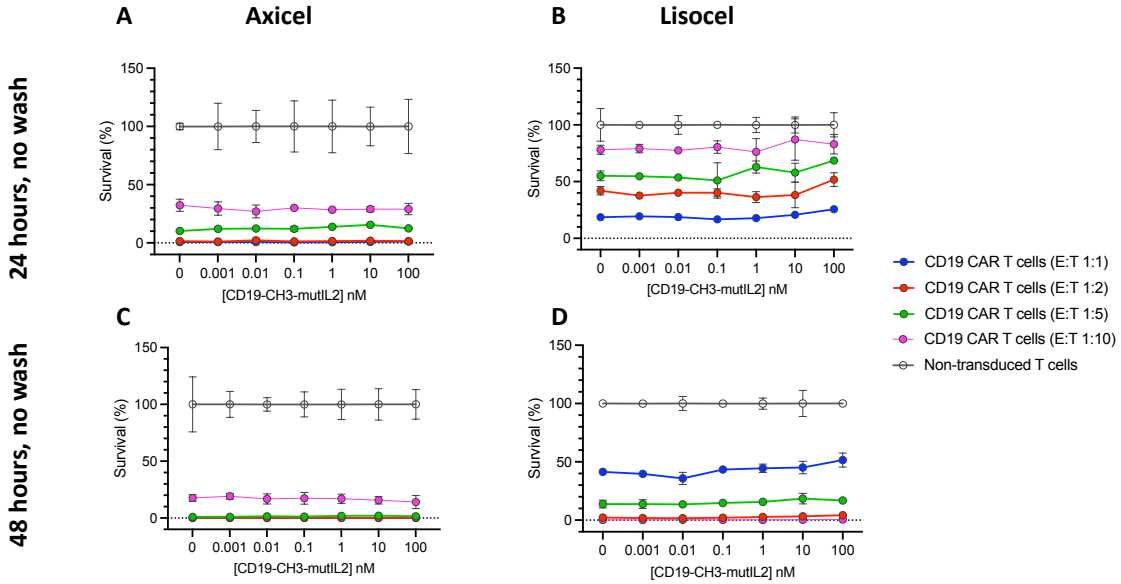

*Figure 14: Killing profile of Axicel and Lisocel against Nalm6 cell, providing insights into their cytotoxic efficacy **A)** quantifies the percentage of survival of Nalm6 cells after 24-hour incubation of Axicel and CD19-CH3-mutIL2 without washing off the CAR-E **B)** showcases the percentage survival of Nalm6 cells following a 24-hour incubation with Lisocel and CD19-CH3-mutIL2 without washing it off **C)** depicts the percentage survival of Nalm6 cells upon incubation with Axicel and CD19-CH3-mutIL2 for 48 hours with no washing of the CAR-E **D)** shows the percentage survival of Nalm6 cells upon 48-hour incubation with Lisocel and CD19-CH3-mutIL2 with no washing*

In **Figure 14A)**, the 24-hour killing profile of Axicel is presented. Notably, even at the highest concentration of CD19-CH3-mutIL2 and the maximal E:T ratio of 1:1, complete cell killing is observed. This effect persists at an E:T ratio of 1:2, with an increment in cell survival as the E:T ratio decreases. **Figure 14B)** depicts the 24-hour condition for Lisocel, revealing minimal blocking at elevated concentrations. Comparatively, Lisocel exhibits inferior killing capacity relative to Axicel.

Figure 14C) portrays Axicel's killing efficacy after 48 hours, demonstrating no blocking phenomenon, with nearly all E:T ratios exhibiting 0% cell survival, except for the 1:10 E:T ratio. **Figure 14D)** illustrates Lisocel's killing profile after 48 hours, where the 1:1 E:T ratio appears to attenuate killing efficacy by approximately 20%. In contrast, other E:T ratios exhibit enhanced killing compared to the 24-hour condition (**Figure 14B)**).

Collectively, the experiment indicates that CAR-E does not induce blocking, even at high E:T ratios. However, a distinction between Axicel and Lisocel is evident, with Axicel displaying superior killing of Nalm6 cells compared to Lisocel.

3.2 In vivo characterization of the CAR-E

The in vitro characterizations of CAR-E have yielded noteworthy outcomes. To substantiate its efficacy in vivo, three experiments were undertaken. The first experiment focused on in vivo expansion, while the second and third experiments involved the injection of mice with Nalm6 and Raji cells, respectively, followed by treatment with CAR-E.

Nalm6 cells, derived from a B cell precursor leukemia cell line originating from an adolescent male, were chosen as the target for the second experiment. Nalm6 cells are frequently employed in CAR-T cell therapy research due to their status as an accessible target.(24) Conversely, Raji cells, established in 1963 from a patient with Burkitt's lymphoma, constitute the target for the third experiment. Raji cells form solid tumors and are recognized as a challenging target for CAR-T cell therapy.(25)

These in vivo experiments aim to further validate the therapeutic potential of CAR-E, particularly in the context of its expansion capabilities and effectiveness against both an easily targetable cell line (Nalm6) and a challenging solid tumor model (Raji).

3.2.1 In vivo expansion

The in vivo expansion experiment is designed to demonstrate the capacity of CAR-T cells to proliferate even in the absence of cancer cells, facilitated by the administered treatment.

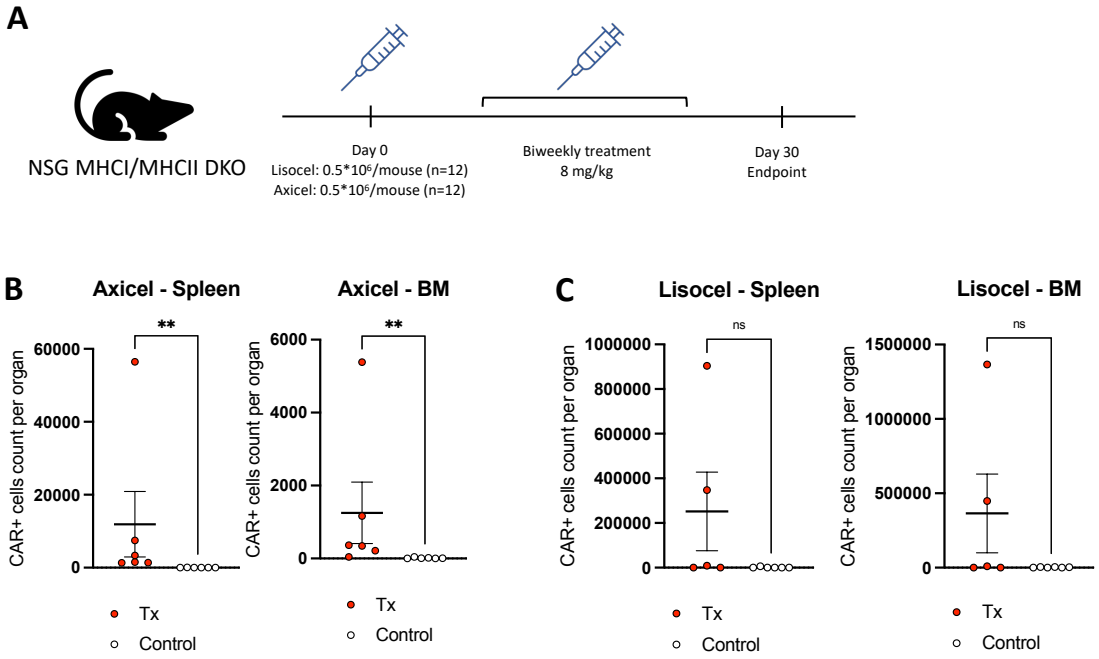

*Figure 15: Expansion of CAR-T cells in the absence of cancer **A)** depicts the timeline of the experiment **B)** showcases the CAR-positive cell count of Axicel in spleen and bone marrow (BM) **C)** depicts the CAR-positive cell count of Lisocel in spleen and BM. p-value >0.05 = ns; p-value 0.01-0.05 = *; p-value 0.001-0.01 = **; p-value <0.001 = ****

In **Figure 15A)**, the experimental timeline is presented. For both Lisocel and Axicel, twelve mice each were injected with $0.5*10^6$ CAR-T cells per mouse. Six mice of each group underwent bi-weekly treatments at a dosage of 8 mg/kg, with the experiment concluding at day 30. **Figure 15B)** illustrates the analysis of the spleen and bone marrow of Axicel-treated mice. A highly significant difference is evident in both organs, with the treatment group exhibiting a higher abundance of CAR-T cells compared to the control group. Conversely, **Figure 15C)** depicts the analysis of the spleen and bone marrow of Lisocel-treated mice. In this case, only two mice displayed an increased level of CAR-T cells, while the sixth mouse succumbed. The observed difference in CAR-T cell levels in Lisocel-treated mice did not reach statistical significance.

These findings suggest that the in vivo expansion of CAR-T cells is robustly supported by Axicel treatment, as evidenced by significantly elevated CAR-T cell populations in both spleen and bone marrow. However, Lisocel treatment exhibited a less consistent impact, with only a subset of mice demonstrating increased CAR-T cell levels, and overall statistical significance was not attained.

3.2.2 Challenging mice with Nalm6

This experiment is designed to elucidate the impact of CAR-E on CAR-T cells, specifically in enhancing their cytotoxic efficacy compared to untreated conditions. As previously stated, Nalm6 cells represent a cancer cell line easily targeted by CAR-T cell therapy.

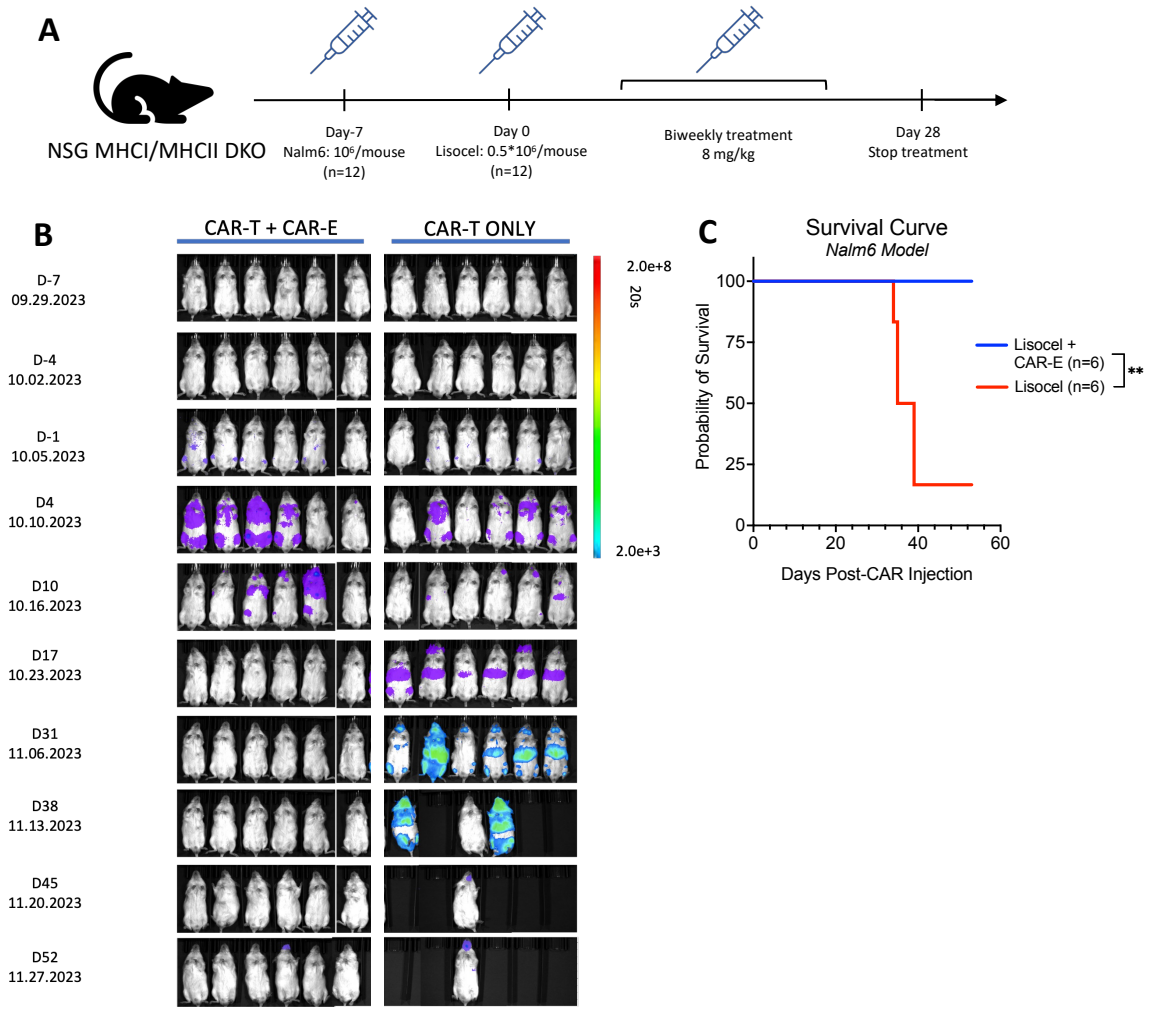

*Figure 16: Mice suffering from Nalm6 cancer cells are treated with Lisocel and CAR-E **A)** outlines the timeline of the experiment **B)** illustrates the BLI of mice which were treated with the CAR-E and without over the span of 52 days **C)** quantifies the probability of survival for the mice challenged with Nalm6. p-value >0.05 = ns; p-value 0.01-0.05 = *; p-value 0.001-0.01 = **; p-value <0.001 = ****

Figure 16A) outlines the experimental timeline: at day -7, 12 mice were injected with 10^6 Nalm6 cells per mouse. At day 0, all mice received an injection of $0.5*10^6$ Lisocel cells per mouse. Six of these mice underwent biweekly treatment with a

dosage of 8 mg/kg, with the treatment concluding at day 28. In **Figure 16B)**, BLI at specified time points reveals distinct tumor signal dynamics. The group receiving both CAR-T cells and CAR-E (CAR-T + CAR-E) exhibits an initial increase in tumor signal at day 4, followed by complete tumor clearance at day 17 without relapse. In contrast, the control group treated solely with CAR-T cells starts developing a tumor signal at day 4, with a progressive increase over time leading to mouse mortality, leaving only one surviving mouse at day 52. **Figure 16C)** presents a survival curve, indicating that the Lisocel + CAR-E group attains a 100% probability of survival, while the control Lisocel group demonstrates a survival probability of approximately 20% by day 40. This substantial difference between the two groups is statistically significant.

In summary, the CAR-E demonstrates a capacity to enhance the performance of Lisocel, as evidenced by improved tumor clearance and increased survival probability in the treated group.

3.2.3 Challenging mice with Raji

This experiment was conducted to demonstrate the capability of CAR-E to significantly enhance the performance of CAR-T cells, leading to the effective clearance of a challenging solid tumor. As previously indicated, Raji cells pose a formidable target for CAR-T cell therapy.

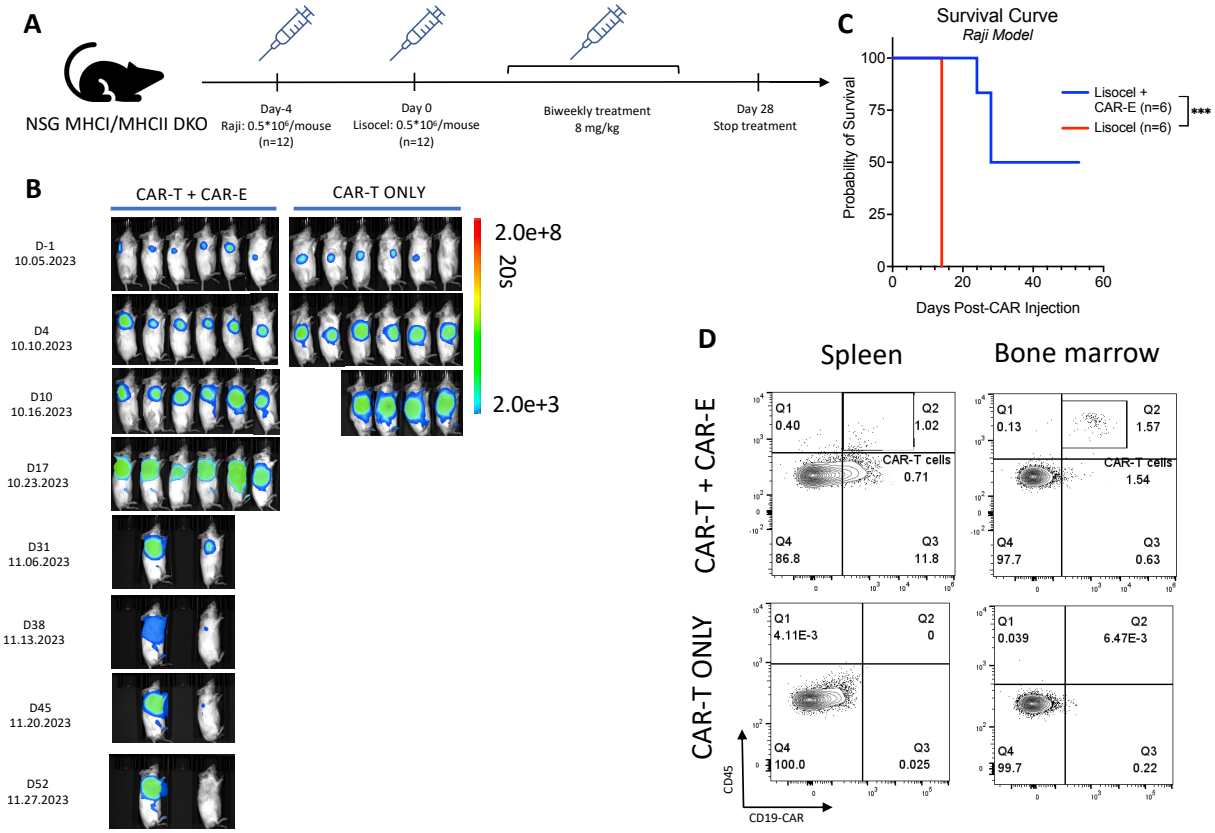

*Figure 17: Mice challenged with Raji cancer cells are treated with Lisocel and CAR-E **A)** outlines the timeline of the experiment **B)** depicts the BLI of the mice treated with CAR-E and without for 52 days **C)** quantifies the probability of survival of mice challenged with Raji **D)** illustrates flow cytometric analysis of spleen and bone marrow. The y-axis represents the expression of CD45, a common leukocyte marker, while the x-axis delineates the expression of CD19-CAR. p-value >0.05 = ns; p-value 0.01-0.05 = *; p-value 0.001-0.01 = **; p-value <0.001 = ****

In **Figure 17A)**, the experimental timeline is presented. At day -4, $0.5*10^6$ Raji cells per mouse were subcutaneously injected into 12 mice. At day 0, $0.5*10^6$ Lisocel cells were administered per mouse, followed by biweekly treatment at a dose of 8 mg/kg of six mice, with the treatment concluding at day 28. **Figure 17B)** displays the BLI of the mice. The CAR-T + CAR-E group exhibited the initiation of tumor burden at day -1, progressively increasing thereafter. By day 31, four mice succumbed to the tumor burden, while one surviving mouse achieved complete tumor clearance. In contrast, the CAR-T-only group displayed a similar initiation of tumor burden at day -1, but the increase was more rapid. On day 10, two mice died, and by day 17, all mice in this group had perished. A noteworthy observation is the accelerated tumor burden progression in the CAR-T-only treated group. **Figure 17C)** presents the survival curve, indicating a 0% probability of survival for the control

group at day 17, while the treatment group demonstrates a 50% probability of survival at day 31. This difference is highly significant. In **Figure 17D)**, a flow cytometric analysis of one mouse from each group is depicted. The x-axis represents the expression of CD19 CAR, and the y-axis represents the expression of CD45. CAR-T cells are expected to be found in quadrant 2. The analyzed organs include spleen, and bone marrow. In the CAR-T + CAR-E group, a percentage between 1 and 2% of CAR-T cells is detectable in each organ. Conversely, no CAR-T cells could be identified in the organs of the CAR-T-only group.

Overall, the CAR-T + CAR-E group exhibited slower tumor burden progression, higher survival rates, and successful tumor clearance compared to the CAR-T-only group. Flow cytometric analysis in **Figure 17D)** confirmed the presence of CAR-T cells in various organs of the CAR-T + CAR-E group, whereas no CAR-T cells were detected in the CAR-T only group. These findings collectively highlight the efficacy of CAR-E in improving CAR-T cell performance against a difficult solid tumor.

4 Discussion

The preceding sections have meticulously scrutinized the in vitro characterizations of the CAR-E, unraveling intricate details regarding binding efficacy, activation capabilities, proliferation dynamics, killing potential, and potential off-target effects. As we transition into the discussion, a meticulous analysis of these findings ensues, encompassing not only their intrinsic mechanistic implications but also the broader context elucidated by in vivo experiments. This comprehensive investigation includes CAR-T cell expansion and challenges with Nalm6 and Raji cells.

Our exploration into the binding affinity of CAR-E constructs to Axicel and Lisocel reveals nuanced patterns indicative of selectivity and specificity. A closer examination of variations in binding affinity among CD19-CH3-mutIL2, CD19-CH3, CD19-CH2-CH3-mutIL2, and BCMA-CH3-mutIL2 unravels the nuanced interplay of these constructs. Particularly noteworthy is the observation of significantly smaller EC50 values for Axicel compared to Lisocel, signifying higher binding affinity. The effective mutation of the IL2 domain, as exemplified by minimal binding of BCMA-CH3-mutIL2 constructs at elevated concentrations, underscores the intricate modulation of receptor interactions.

The activation potential of CAR-E, assessed through pSTAT5 and CD69 assays, undergoes meticulous scrutiny in this discussion. Comparative analyses with Tecleukin, a benchmark IL2 variant, are integrated to discern the unique contributions of CAR-E in modulating the activation dynamics of CAR-T cells. Emphasis is placed on the temporal evolution of activation signals at both 30 minutes and 24 hours, revealing consistent trends for both Axicel and Lisocel. CD19-CH3-mutIL2 and CD19-CH2-CH3-mutIL2 consistently exhibit the highest activation levels in both pSTAT5 24-hour and CD69 24-hours assays. Furthermore, a comprehensive cytokine profile analysis showcases an increase in IFNγ and TNFα.

The proliferation capabilities of CAR-E, demonstrated through proliferation assays, indicate a notable proliferative response, with Axicel and Lisocel exhibiting proliferation, albeit with attenuation at high concentrations due to an extended incubation

period of 4 days. The evaluation of CAR-E's impact on killing capabilities, conducted through a high-density killing assay, reveals minimal blocking at high concentrations and an enhanced killing ability of Axicel compared to Lisocel.

Extending our analysis beyond in vitro assessments, the discussion encapsulates in vivo data concerning CAR-T cell expansion and challenging mice with Nalm6 and Raji cells. Insights from the in vivo expansion experiments bridge observed in vitro functionalities with potential translational applications of CAR-E in clinical settings. While Axicel exhibits a significant expansion compared to the control group, Lisocel, although showing no significant difference, manifests elevated CAR-T cell count in two mice, with one unfortunate incidence of mortality.

Challenging mice with Nalm6 proves highly successful, leading to tumor clearance in all treated mice, while control mice succumb to the challenge. This experiment attains a high level of statistical significance. Similarly, challenging mice with Raji cells results in remarkable success, with all control mice perishing, while treated mice demonstrate tumor clearance, accompanied by the presence of CAR-T cells in various organ sites. This experiment yields a very high level of statistical significance.

Observations of off-target effects on non-transduced T cells are situated within the comprehensive framework of CAR-E safety, a crucial aspect necessitating scrutiny by regulatory bodies such as the FDA. A meticulous analysis reveals minimal off-target effects, predominantly discernible at elevated concentrations. The abbreviated half-life of CAR-E, enabling swift excretion within a span of hours, serves as a pivotal element accentuating its safety profile. The importance of these safety considerations gains heightened relevance, especially in the context of advanced therapies like CAR T cell therapy, where regulatory evaluation by entities such as the FDA plays a paramount role.(26)

The dose-dependent behavior of CAR-E emerges as a pivotal point of discussion, particularly in the context of potential clinical applications. Exploration of implications for optimizing therapeutic interventions, considering varying concentrations of CAR-E, is undertaken. The clinical relevance of these findings offers insights into their potential impact on the advancement of CAR-T cell therapy.

In summary, this comprehensive discussion seamlessly integrates in vitro findings with in vivo data, providing a holistic understanding of the multifaceted functional implications of CAR-E constructs. The synergistic alignment of mechanistic insights and translational perspectives contributes to our comprehensive understanding of the dynamic interplay essential for advancing the efficacy and safety of CAR-T cell therapies.

List of References

1. Allemani C, Weir HK, Carreira H, Harewood R, Spika D, Wang XS, et al. Cancer. Our World in Data [Internet]. 2015 Jul 3 [cited 2023 Oct 21];385(9972):977–1010. Available from: https://ourworldindata.org/cancer

2. Blood Cancer (Hematological Malignancies) | Penn Medicine [Internet]. [cited 2023 Oct 21]. Available from: https://www.pennmedicine.org/cancer/navigating-cancer-care/programs-and-centers/hematological-malignancies-program#:~:text=Your%20treatment%20options%20may%20include,called%20CAR%20T%20cell%20therapy

3. Worldwide cancer data | World Cancer Research Fund International [Internet]. [cited 2023 Oct 21]. Available from: https://www.wcrf.org/cancer-trends/worldwide-cancer-data/#:~:text=Find%20information%20about%20world%20cancer,and%208.8%20million%20in%20women.

4. Mohanty R, Chowdhury CR, Arega S, Sen P, Ganguly P, Ganguly N. CAR T cell therapy: A new era for cancer treatment (Review). Oncol Rep [Internet]. 2019 Dec 1 [cited 2023 Dec 11];42(6):2183–95. Available from: http://www.spandidos-publications.com/10.3892/or.2019.7335/abstract

5. June CH, O'Connor RS, Kawalekar OU, Ghassemi S, Milone MC. CAR T cell immunotherapy for human cancer. Science (1979) [Internet]. 2018 Mar 23 [cited 2023 Jul 24];359(6382):1361–5. Available from: https://www.science.org/doi/10.1126/science.aar6711

6. Larson RC, Maus M V. Recent advances and discoveries on the mechanisms and functions of CAR T cells. Nat Rev Cancer [Internet]. 2021 Mar 1 [cited 2023 Aug 20];21(3):145. Available from: /pmc/articles/PMC8353572/

7. Benmebarek MR, Karches CH, Cadilha BL, Lesch S, Endres S, Kobold S. Killing Mechanisms of Chimeric Antigen Receptor (CAR) T Cells. International Journal of Molecular Sciences 2019, Vol 20, Page 1283 [Internet]. 2019 Mar

14 [cited 2023 Aug 25];20(6):1283. Available from: https://www.mdpi.com/1422-0067/20/6/1283/htm

8. Maakaron JE, Hu M, Jurdi N El. Chimeric antigen receptor T cell therapy for cancer: clinical applications and practical considerations. [cited 2023 Aug 19]; Available from: http://dx.doi.org/10.1136/

9. Tokarew N, Ogonek J, Endres S, von Bergwelt-Baildon M, Kobold S. Teaching an old dog new tricks: next-generation CAR T cells. Br J Cancer. 2019 Jan 8;120(1):26–37.

10. Hong M, Clubb JD, Chen YY. Engineering CAR-T Cells for Next-Generation Cancer Therapy. Cancer Cell [Internet]. 2020 Oct 12 [cited 2023 Aug 19];38(4):473–88. Available from: http://www.cell.com/article/S1535610820303664/fulltext

11. Cappell KM, Kochenderfer JN. Long-term outcomes following CAR T cell therapy: what we know so far. Nat Rev Clin Oncol [Internet]. 2023 [cited 2023 Jul 21];20:359–71. Available from: https://doi.org/10.1038/s41571-023-00754-1

12. Sengsayadeth S, Savani BN, Oluwole O, Dholaria B. Overview of approved CAR-T therapies, ongoing clinical trials, and its impact on clinical practice. 2021; Available from: https://onlinelibrary.wiley.com/doi/10.1002/jha2.338,

13. Boettcher M;, Joechner A;, Li Z;, Yang SF;, Schlegel P, Chauncey R, et al. Citation: Clinical Medicine Development of CAR T Cell Therapy in Children-A Comprehensive Overview. J Clin Med [Internet]. 2022; Available from: https://doi.org/10.3390/jcm11082158

14. Sterner RC, Sterner RM. CAR-T cell therapy: current limitations and potential strategies. Sterner and Sterner Blood Cancer Journal [Internet]. 2021 [cited 2023 Oct 19];11:69. Available from: https://doi.org/10.1038/s41408-021-00459-7

15. Shah NN, Fry TJ. Mechanisms of resistance to CAR T cell therapy. Vol. 16, Nature Reviews Clinical Oncology. Nature Publishing Group; 2019. p. 372–85.

16. Choi S Il, Yin J. Prospective approaches to enhancing CAR T cell therapy for glioblastoma. 2022;

17. Eisenberg V, Hoogi S, Shamul A, Barliya T, Cohen CJ. T-cells “à la CAR-T(e)” – Genetically engineering T-cell response against cancer. Adv Drug Deliv Rev. 2019 Feb 15;141:23–40.

18. Zhang Q, Hresko ME, Picton LK, Su L, Hollander MJ, Nunez-Cruz S, et al. A human orthogonal IL-2 and IL-2Rβ system enhances CAR T cell expansion and antitumor activity in a murine model of leukemia. Sci Transl Med [Internet]. 2021 Dec 22 [cited 2023 Dec 11];13(625):6986. Available from: https://www.science.org/doi/10.1126/scitranslmed.abg6986

19. Moghanloo E, Mollanoori H, Talebi M, Pashangzadeh S, Faraji F, Hadjilooei F, et al. Remote controlling of CAR-T cells and toxicity management: Molecular switches and next generation CARs. Transl Oncol. 2021 Jun 1;14(6):101070.

20. Quayle SN, Girgis N, Thapa DR, Merazga Z, Kemp MM, Histed A, et al. Cue-101, a novel E7-pHLA-IL2-Fc fusion protein, enhances tumor antigen-specific T-cell activation for the treatment of HPV16-driven malignancies. Clinical Cancer Research [Internet]. 2020 Apr 15 [cited 2023 Dec 11];26(8):1953–64. Available from: https://dx.doi.org/10.1158/1078-0432.CCR-19-3354

21. Leonard WJ, Lin JX. Cytokine receptor signaling pathways. Journal of Allergy and Clinical Immunology. 2000 May 1;105(5):877–88.

22. Ziegler SF, Ramsdell F, Alderson MR. The activation antigen CD69. Stem Cells [Internet]. 1994 Jan 1 [cited 2024 Jan 14];12(5):456–65. Available from: https://dx.doi.org/10.1002/stem.5530120502

23. Slifka MK, Whitton JL. Activated and Memory CD8+ T Cells Can Be Distinguished by Their Cytokine Profiles and Phenotypic Markers. The Journal of Immunology [Internet]. 2000 Jan 1 [cited 2024 Jan 14];164(1):208–16. Available from: https://dx.doi.org/10.4049/jimmunol.164.1.208

24. Charkhizadeh S, Imani M, Gheibi N, Shabaani F, Nikpajouh A, Rezvany MR. In Vitro Inhibitory Effect of Recombinant Human Calprotectin on Nalm6 Leukemia Cell Line. Anticancer Agents Med Chem [Internet]. 2020 Mar 31 [cited 2024 Jan 14];20(8):951–62. Available from: https://pubmed.ncbi.nlm.nih.gov/32228430/

25. Apter AJ, Bender BG, Rand CS. 091 – Adherence [Internet]. Middleton's Allergy: Principles and Practice: Eighth Edition. 2014 [cited 2024 Jan 14]. 1471–1479 p. Available from: http://www.sciencedirect.com:5070/book/9780323085939/middletons-allergy

26. Zheng PP, Kros JM, Li J. Approved CAR T cell therapies: ice bucket challenges on glaring safety risks and long-term impacts. Drug Discov Today. 2018 Jun 1;23(6):1175–82.